SPRAY AND COMBUSTION CHARACTERISTICS OF ACETONE-BUTANOL-ETHANOL AND DIESEL IN A CONSTANT VOLUME CHAMBER AND A DIESEL ENGINE

BY

TIMOTHY LEE

THESIS

Submitted in partial fulfillment of the requirements
for the degree of Master of Science in Mechanical Engineering
in the Graduate College of the
University of Illinois at Urbana-Champaign, 2015

Urbana, Illinois

Adviser:

Professor Alan Hansen

Abstract

Recent research has shown that butanol, instead of ethanol, has the potential of introducing a more suitable blend in diesel engines. This is because butanol has properties similar to current transportation fuels in comparison to ethanol. However, the main downside is the high cost of the butanol production process. Acetone-butanol-ethanol (ABE) is an intermediate product of the fermentation process of butanol production. By eliminating the separation and purification processes, using ABE directly in diesel blends has the potential of greatly decreasing the overall cost for fuel production. This could lead to a vast commercial use of ABE-diesel blends on the market. Research has been done in the past five years concerning spray and combustion processes of both neat ABE and ABE-diesel mixtures. Additionally, different compositions of ABE mixtures had been characterized with a similar experimental approach.

This thesis reviews the production of ABE and characterization of its spray and combustion processes. The results obtained during the recent four years will also be presented. The main focus of this paper is to review the efforts made in fundamental spray research under quasi-steady flow field environments provided by a high-pressure, high-temperature constant volume chamber. In-cylinder pressure traces were calculated to derive apparent heat release rates, high-speed Mie-scattering images were acquired to characterize liquid spray penetration, and natural flame luminosity was also captured to depict spatial and temporal soot distribution. It is observed that the acetone content has a major influence in the combustion behavior of the ABE mixture. An increased content of acetone will lead to a significantly advanced combustion phasing. Butanol, as another important species in the ABE mixture, is able to compensate the advancing effect caused by acetone and ethanol. More importantly, butanol can increase the

overall energy density of the mixture, which makes the property of the mixture closer to that of current transportation fuels. In addition, the underlying challenges faced in this area of research are described.

Additionally, the performance and emissions of acetone-butanol-ethanol (ABE)/diesel mixtures in an AVL 5402 single cylinder diesel research engine under various engine operating conditions were investigated in this study. The experiments were conducted at three different speeds (1200, 1500, and 2000 RPM) and different injection quantities (loads) (15, 20, and 25 mg/cycle).

The fuels tested in these experiments were pure diesel, ABE10, and ABE20. The acetone-butanol-ethanol (ABE) was blended in a 3:6:1 ratio. ABE10 and ABE20 consist of 10% acetone-butanol-ethanol mixture and 90% diesel by volume and 20% ABE is mixed with 80% diesel by volume, respectively.

The results showed a promising future for ABE-diesel mixtures as an alternative transportation fuel. There was improved thermal efficiency even with relatively small ABE blending ratios and a slight reduction in power output due to the lower energy density. There was an overall retarded combustion phasing, including longer ignition delay time, retarded CA50 timing, peak pressure timing, and end of combustion timing. Accelerated heat release during CA10~CA50 indicates a higher degree of premixed combustion. Overall soot emissions were lower and NOx emissions were higher for ABE-containing fuels at the same load and timing conditions. Tuning the injection timing would be helpful for the reduction of NOx to a degree that is even lower than that of diesel.

With proper tuning of the injection quantity and injection timing, adopting ABE-diesel mixtures has the potential of improving efficiency and reducing emissions at the same time.

Considering the low cost of ABE production compared to other kinds of bio-fuels, ABE could become a possible alternative to the current fuel additives.

Acknowledgements

I wish to thank the University of Illinois at Urbana-Champaign along with the College of Engineering and Department of Mechanical Science and Engineering department for this opportunity to further my education. I would also like to thank my Professor, Dr. Alan Hansen, for giving me direction in my research.

I give thanks and love to my parents Chia-fon Lee and Yu-yu Lee for supporting me in my decisions to pursue a Master's Degree. My sister, Christine Lee, has also been a great encouragement.

I thank my laboratory co-workers, Wu Han, Yilu Lin, and Karthik Nithyanadan, who helped my research greatly. Without them, this thesis would not be possible.

Finally, I thank Zikang Tong and those at the Vineyard Church who have been a continuous encouragement to me.

Table of Contents

List of Tables

List of Figures

Chapter 1

Introduction

Recent growing concerns over the economic and environmental viability of gasoline, diesel, and fossil fuels have driven the investigation of biofuels. Biofuels, fuels created from agricultural sources, offer the exciting possibility of "renewability" in the sense that the biofuels can be regenerated by the eco-system using the combustion products of the fuels. In this way, power generation can be achieved with significantly reducing its contribution to climate change. Currently, research in this area has developed along two completely independent lines with the dominant trend being the production of pure chemicals from agricultural processes. There has been a significant amount of work focused on the "upstream", which includes the biological processes that produce these pure fuels in an efficient and environmentally friendly way from appropriate raw materials. Lately, there have been rapid developments studying the "downstream", which are the mechanical and chemical processes that relate to the application of bio-fuels to the power generation and transportation sectors.

Among these biofuels, oxygenated compounds (which include butanol, ethanol, methanol, and ethers or methyl or ethyl esters), have been considered as an additive for conventional fuels [1]. Recent research has shown that butanol, instead of ethanol, has the potential of being a more suitable blend in diesel engines. This is because butanol has properties similar to current transportation fuels in comparison to ethanol. Butanol can be produced using renewable biomass resources such as whey, permeate, corn, wood hydrolysate, starch and other monomer sugars.

Bio-butanol commonly uses the microorganism *Clostridium acetobutylicum* to ferment the starch or sugars to butanol. During this bacterial fermentation process, acetone, n-butanol,

and ethanol are created in volumetric percentages of approximately 22-33%, 62-74%, and 1-6% respectively, which is roughly a 3:6:1 ratio [2, 3]. From there, the butanol is extracted from the mixture. Unfortunately, the high cost of the butanol production process limits the usage in current transportation.

However, if the intermediate product of acetone-butanol-ethanol (ABE) could be used for clean combustion instead of pure butanol, the separation costs for bio-butanol could be mitigated. As a result, a large amount of time and money could be eliminated in the production of an alternative additive for diesel. The goal of this study is to explore the spray characteristics and combustion processes of acetone-butanol-ethanol in a constant volume chamber and in a diesel engine.

Chapter 2

Literature Review & Theory

2.1 Production of ABE Mixtures

A recently emerging bio-fuel is butanol, which was recently produced through an anaerobic process involving a fermentation microorganism. Renewable biomass resources such as whey permeate, corn, wood hydrolysate, starch and other monomer sugars can be used to produce butanol. *Clostridium acetobutylicum* is the most commonly used microorganism in the industry to convert the starch or sugars to butanol and *clostridium beijerinckii* is another newly developed strain which has a higher concentration of butanol in the fermentation [4-6]. Acetone-butanol-ethanol (ABE) fermentation, the fermentation process in which a 3:6:1 acetone: butanol: ethanol mixture, referred to as baelene, is obtained [5, 7]. The main problem of the fermentation is the butanol toxicity to the culture, which ideally should be reduced. As a result, it is necessary to remove the solvent from the fermentation vessel for simultaneous production. Besides the traditional distillation method, several recovery techniques have been developed for the butanol extraction from the fermentation broth including adsorption, liquid-liquid extraction, perstraction, pervaporation, reverse osmosis, and gas stripping [8]. ABE fermentation has been of interest as an alternative method for generating these chemicals, rather than relying on petrochemicals for their production. This interest has been recently accentuated by the high cost of petrochemicals and the drive towards less dependence on petroleum. At present, the genome sequence for the microorganisms that produce the solvents is being determined and, once available, will allow investigators to unravel the general principles of solvent production. This will ultimately lead to a rational metabolic engineering-based approach for the development of

second-generation strains with characteristics that are optimized for the production of biosolvents or bio-fuels from renewable sources.

Acquiring the pure butanol from the fermentation solvent is based on the combination of acetone-butanol-ethanol distillation [6]. The cost of recovering butanol through distillation is high because of its boiling point of 118°C. This leads to a high-energy input in the distillation process as bio-butanol contains mainly 1-butanol and small quantities of the other isomers that have different boiling points. Being able to make use of the ABE mixture as a bio-fuel, referred to as baelene, without having to execute a further distillation step will lead to substantial cost and energy savings. This can overcome the disadvantages of the high cost of butanol production from ABE fermentation and thus make ABE fermentation more attractive due to its economic efficiency. Several important characteristics of the combustion processes in the engine cylinder (heat release, main combustion products) exhibit very little sensitivity to precise molecular structure of the fuel [9]. For this reason, it should be possible to operate engines in a clean and efficient manner using intermediate products of the fermentation process (like baelene) without the need to produce pure chemicals (like butanol or ethanol). However, the possibility of operating with a fuel blend raises the question of blend composition optimization, i.e. “guiding” the baelene production process towards the proportion of acetone/ butanol/ ethanol that will be optimal in terms of both cost-efficient production and clean and efficient performance.

2.2 ABE Component Characteristics

The physical and chemical properties of the species concerned with ABE research are tabulated. Additionally, some basic mixture properties of the blended fuels are calculated and shown in Table 2.1. From the table it can be seen that all single components of the ABE mixture

show higher latent heat, higher auto-ignition temperature, lower LHV, and lower boiling point. When the ABE mixture is added into diesel, the volatility of the mixture is improved. A retarded auto-ignition can also be expected due to the limitation of the auto-ignition temperature and the effect of vaporization cooling.

2.2.1 Acetone

Acetone is the most volatile species among the ABE mixture, with the lowest boiling point and the highest saturation pressure (Table 2.1). Experimental works on pure acetone combustion are quite rare because acetone is essentially deemed to be an intermediate product during the combustion of hydrocarbons and oxygenates. Also, it is often used as a tracer to facilitate PLIF diagnostics for fuel distribution and temperature [14, 15, 16].

2.2.2 Butanol

Butanol has four different forms of isomer: n-butanol, sec-butanol, iso-butanol and tert-butanol. Although they share the same formula, due to different structures of these isomers, the physical properties (boiling point, density, viscosity, etc.) are quite distinct. Wu and Law [17] further discovered that the isomers also have quite different laminar flame speed and Markstein length, with n-butanol showing the maximum laminar flame speed. Through reaction path analysis, the authors identified that the other three isomers will be turned into some intermediate species which are more stable and are of low reactivity.

Liu et al. [18, 19] investigated the spray liquid penetration length, combustion heat release rate and soot emission characteristics of pure n-butanol in comparison with biodiesel. Compared to biodiesel, n-butanol exhibits a higher normalized peak combustion pressure, which

is a result of larger quantity of heat released in a shorter time period, indicating higher combustion efficiency in constant volume combustion. This is due to the higher energy conversion efficiency and lower heat loss. In accordance, the natural flame luminosity of n-butanol is lower than that of diesel, meaning there is a more complete combustion.

Liu and Li [20-22] investigated how n-butanol affected diesel and biodiesel mixtures. These n-butanol, diesel, and bio-diesel blends were tested inside a constant volume chamber to investigate the liquid spray and combustion of the fuels. The authors found that when the ambient temperature was higher, the spray jet penetration was shortened due to a faster liquid evaporation.

Additionally, with more n-butanol added to the mixture, the spray penetration length was also reduced. Furthermore, microexplosions, which are caused by internal gasification of a liquid mixture with different volatilities and boiling points, increased with the increase of n-butanol. This is due to the higher volatility of n-butanol in comparison to diesel and biodiesel. The microexplosions in turn also reduce spray penetration. Liu also discovered that with the addition of more n-butanol, the spray jet angle of the fuel blend increased. This is because after adding the n-butanol, the viscosity and surface tension are reduced. On the other hand, the diffusion rate and the air entrainment of the spray were both enhanced. As a result, the droplet has an easier time atomizing into uniform droplets. In other words, adding appropriate amounts of n-butanol to a biodiesel and diesel blend can acquire similar spray characteristics as diesel. This in turn can effectively reduce hydrocarbon and particulate emissions.

2.2.3 Ethanol

Liu et al. [23] compared the impacts of ethanol and butanol addition in soybean biodiesel fuel. The alcohols were blended with diesel in a volumetric ratio of 1:4. An optical accessible

constant volume chamber was used to conduct a detailed comparative investigation on the spray, combustion and soot formation/ oxidation processes of both fuel blends. Some major differences between impacts introduced by ethanol and butanol include: the heat release mode for ethanol-biodiesel blends is more "violent" with shorter combustion duration and higher peak combustion pressure, indicating a potentially higher thermal efficiency. On the other hand, this may also mean that ethanol addition will cause an increased level of NO_x emission; the ignition timing for butanol-biodiesel blend is typically earlier than that of ethanol-biodiesel blends under high temperature conditions, i.e. 1000K and 1200K in this paper, which is in accordance with the observations mentioned earlier. Another merit of ethanol is that it has a less sooting tendency than butanol. However, this has a compromised result from the lower heating value and energy density of ethanol.

2.3 ABE with Fuels

2.3.1 Gasoline

Researchers have investigated the application of ethanol-diesel in engine experiments [24, 25]. Common conclusions include a decrease in engine torque output, which corresponds to the decrease of energy content. Additionally, in terms of emissions, ethanol content in diesel can lead to a decrease in PM emissions.

Nithyanandan et al. [26-30] have also studied the performance and emissions of ABE-gasoline blends on an SI engine. In the case of pure gasoline, ABE20 (ABE in a ratio of 3:6:1 and mixed with gasoline in a 20% ratio), and ABE40, it was found that ABE20 featured a shorter ignition delay and an advancement of the mass fraction burned (where 50% of the mass fraction of the fuel was burned). ABE40 displayed a deteriorated combustion quality due to the high

latent heat of vaporization of ABE and combustion phasing [26]. Due to the lower energy content of the blends, BSFC (brake specific fuel consumption) increased with increasing ABE fraction.

Blends of pure ethanol-free gasoline and ABE were combusted in a port-fuel injected spark ignition engine [27]. ABE0-ABE80 ratios were combusted in these tests. Overall, the ABE ratios displayed lower peak cylinder pressure than that of gasoline with the exception of ABE80. Blends with a lower ABE content featured a slightly longer ignition delay and a retarded 50% (MFB) location and once again, ABE 80 was the exception with shorter ignition delay. BSFC increased with increasing ABE fractions, much like the other paper's results. Emission data showed that the CO decreases and unburned hydrocarbons (UHC) increased and then decreased for all blends.

Additionally, ABE in ratios of 3:6:1 and 6:3:1 were blended into ethanol-free gasoline in a volumetric ratio of 70% gasoline and 30% ABE. These blends were combusted in a port-fueled injected spark ignition engine [28]. In-cylinder pressure data showed that the peak pressure of the ABE blends was higher than that of pure ethanol-free gasoline. ABE30(3:6:1) showed advanced combustion phasing and ABE30(6:3:1) displayed similar combustion phasing to pure gasoline. ABE30(3:6:1) showed the highest value for the BSFC and ABE30(6:3:1) showed the lowest. This conclusion may show that ABE(6:3:1) could be better in regards to engine combustion. No major changes were noticed in the NO_x emissions. ABE30(3:6:1) had higher CO emissions and lower UHC than that of gasoline while ABE30(6:3:1) had increased UHC and its CO emissions were equal to that of gasoline.

Zhang et al. [29] compared the effects of high-alcohol-content gasoline blends in an SI-engine. The fuels studied included 85% ethanol, butanol, and ABE blended with 15% gasoline

by volume (referred to as E85, B85, and ABE 85 respectively). E85 had the highest in-cylinder pressure and B85 had the lowest. Under stoichiometric conditions, both ignition delay and combustion durations of the four fuels are in the same sequence of B85>gasoline>ABE85>E85. When compared with gasoline, all the alcohol-containing fuels had slightly lower brake thermal efficiency and higher BSFC under stoichiometric conditions. The alcohol-containing fuels all had lower NO_x emissions.

Li et al. [30] compared the effects of water containing ABE blends in a spark ignition engine. In this paper, ABE29.5W0.5 (29.5% vol.% ABE, 0.5% water, and 70% gasoline blend), ABE30, and pure ethanol-free gasoline blends were tested. ABE29.5W0.5 presented a higher brake thermal efficiency and a similar BSFC relative to pure gasoline. It also showed a longer ignition delay and combustion duration. The amount of NO_x and CO decreased, while the UHC increased for the ABE29.5W0.5.

These preliminary combustion tests of ABE-gasoline in an SI engine were successful because there were no major complications that occurred. They observed that with further optimizations in combustion phasing for ABE and study of the properties of ABE, the optimal ratio between gasoline and ABE could be found.

2.3.2 Diesel

Chang et al. [31] studied the effects of ABE in a diesel engine generator fueled with diesel. Their ABE blend was prepared in a volumetric ratio of 5:14:1 (A:B:E) and were blended with water and diesel in various ratios. Based on their gravitational and centrifugal stability tests, ABE-diesel fuel remained in a clear stable phase when it contained small amounts (0.5-1% vol.) of water. The high oxygen content of the water aided the combustion processes in the ABE-diesel blends and resulted in a more complete combustion. By using ABE20W0.5 in the diesel

engine, there was an increase of 3.26-8.56% than that of pure diesel. The amount particulate matter and NOx decreased significantly. They concluded that ABE20W0.5 diesel is a good alternative to pure diesel.

Chang also tested ABE fuel blends with biodiesel and diesel on a diesel engine to uncover the NOx-PM trade-offs [32]. They studied the effects of regular diesel, biodiesel and diesel blends, and water-containing ABE-diesel-biodiesel blends. Even though the addition of water-containing ABE had a higher BSFC, the high oxygen concentration resulted in better combustion, which offset the lower heating value. These values led to better brake thermal efficiencies in comparison to biodiesel and diesel. Biodiesel-diesel blends and ABE-biodiesel-diesel blends both had lower PM emissions than regular diesel, but biodiesel-diesel blends had higher NOx emissions. On the other hand, ABE-biodiesel-diesel had lower NOx emissions.

Zhou et al. [33] studied the characteristics of different percentages of acetone-butanol-ethanol and diesel blends at low temperature conditions in a constant volume chamber. In the study the ABE blend was kept at a volumetric ratio of 30%, 60%, and 10% by volume of acetone, butanol, and ethanol respectively. The ABE blend was then blended with diesel in ratios of 50% and 80% volume. The fuels were then combusted at 800 K and 1200 K combustion temperatures. In-cylinder pressure was recorded with a pressure transducer and natural luminosity was recorded with high speed imaging. Laser diagnostics were used to provide crucial fundamental information of the fuel's combustion characteristics. It was found that under the low ambient temperature of 800 K, the ABE fuels had extremely low soot luminosity. The ABE-diesel blends had higher oxygen content in comparison to pure diesel, which led to enhanced soot oxidation and consequently lower soot luminosity under all tested conditions. The ABE-diesel blends have longer delay and flame lift off length. This allowed for

more air entrainment upstream of the spray along with better air-fuel mixing. The ABE fuels produced a flameless combustion that lead to extremely low soot luminosity. Additionally, it was discovered that the latent heat of the ABE-fuel blends was higher than diesel, which means that a higher evaporative cooling effect is expected. This would lower the adiabatic flame temperature along with NOx emissions. In low temperature combustion conditions, the evaporative cooling helps suppress the soot formation.

Additionally, Zhou et al. [34] studied the characteristics of acetone-butanol-ethanol-diesel blends in a 20% ABE and 80% diesel by volume, referred to as ABE20. The ABE blend composed of a volumetric ratio of 30%, 60%, and 10% of acetone, butanol, and ethanol respectively. The prepared ABE was set in a test tube at 25°C and 1 atm for 14 days in a stability test. Afterwards, since the ABE did not show any separation, they burned the ABE-diesel blends at a low ambient temperature condition of 800 K and low ambient oxygen of 11%. In comparison to pure diesel, ABE20 presented better combustion efficiency. The ABE-diesel blends had longer ignition delay and flame lift-off length compared to pure diesel in all tests. Once again, ABE-diesel blends could achieve flameless combustion under low ambient conditions since no soot luminosity was detected. This indicated that the soot formation was severely inhibited.

With these studies conducted, it can be seen that ABE is a very promising alternative fuel to be directly used in diesel engines.

2.4 Conventional Diesel Combustion

The fundamental aspects of direct injection diesel engines must be studied as it is the most prevalent and relates to the test engine used in this study. A basic diesel engine operating

description is given here. Air is forced in the cylinder and compressed, creating a high pressure and temperature environment. Fuel is injected into the cylinder as the piston approaches top dead center (TDC). The fuel partially atomizes and vaporizes before igniting. The combustion from this ignition can vary widely, as it depends on the amount of mixing before the fuel self-ignites.

As a result, diesel combustion is considered a highly complex phenomenon from its unsteady and heterogeneous nature. Since conventional metal engines lack in optical access, it is difficult to study what goes on in the cylinder during combustion. In-cylinder pressure transducers are used to provide some general information on the heat release rate. The data gathered from the pressure transducers can be used to calculate the apparent heat release rate, taking into account the heat transfer through the combustion chamber walls, by using analysis of the first law of thermodynamics. Complex calculations have been made possible through massive amounts of literature on the subject, as described in [35].

A typical heat release rate plot for a direct injection diesel engine is shown in Figure 2.1. The heat release rate process can be divided into four main parts. The first part consists of the period after the start of injection (SOI), but the time before the start of combustion is known as the ignition delay. Fuel atomization and vaporization occurs during this phase, which results in a dip into the negative side in the heat release rate diagram due to the energy required for vaporization. The rapid increase in the heat release rate after that characterizes the premixed combustion phases. The period that follows the premixed combustion phase is where the mixed combustion occurs. During this time, the heat release rate is controlled by the remaining fuel-air mixture which decreases over time as kinetic rates slow due to the expansion process and the resulting lower temperatures. This region is called the late combustion phase.

Unfortunately, additional information beyond the in-cylinder pressure and calculated heat release rate is hard to obtain from an ordinary engine. Alternative methods in simulating an engine, such as constant volume chambers and optically accessible diesel engines, have enabled much more insight in the combustion process through a variety of techniques such as combustion imaging and laser diagnostics.

The primary pollutants from the diesel combustion process are NOx and particulate matter containing soot. Since diesel engines have an overall fuel-air ratio that is stochiometrically lean, emissions of carbon monoxide and unburned hydrocarbons are generally rather small. As the air-fuel ratio approaches stoichiometric conditions, however, these emissions become more significant and need to be accounted for.

Nitrogen oxide mechanisms are relatively well known and many sources have been compiled in various papers such as this one [36]. The most prevalent nitrogen oxide would be nitric oxide (NO). In combustion, there are three major sources of NO: the fuel NO mechanism, prompt NO mechanism and thermal NO (Zeldovich) mechanism. The fuel NO mechanisms consist of the oxidation of nitrogen containing organic compounds found in fossil fuels. Prompt NO can be formed in low temperature, fuel rich conditions. The thermal NO mechanism is composed of three reactions, whose rate constants vary over a wide range of temperature and can be accurately measured. An equation can be written using these reactions for the maximum NO formation rate. The final equation shows that the rate of formation for NO is more dependent on burned gas temperature rather than the oxygen concentration in the burned gas. The NO formed in internal combustion engines begins to decompose after it is formed. Yet when the piston expands and the temperature in the cylinder reduces, the decomposition of NO is frozen and the remaining NO is ejected out the exhaust. In the case of diesel engines, the high temperature

burned gases mix with the remaining cooler air, which causes the temperature in the cylinder to reduce to a greater extent than gasoline engines. As a result, relatively more NO is emitted in the exhaust due to lower decomposition of the NO.

Soot formation in diesel engines is fairly complicated and not well understood. In the locally rich region of combustion where high temperature causes thermal cracking of the fuel is where soot particles are thought to be formed. The general consensus is that the molecular precursor of soot forms during pyrolysis [37], or the process of breakdown and rearrangement of the fuel molecules. These soot particles are generated through condensations, polymerization, and dehydrogenation from PAH created by the pyrolysis. Gas phase species, such as acetylene and PAH help the newly-formed soot particles to grow in size. At the same time coagulation takes place as the particle-particle collisions cause soot particles to stick together. These amorphous soot particles convert into a more graphene-like carbon material. These soot particles then go through an oxidation process. Soot formation is prominent during the initial combustion phase, premixed combustion, and beginning of diffusion combustion. In the later periods of the cycle, soot oxidation dominates. Depending on the size of the particles, the soot oxidation can be controlled by either the surface diffusion or the kinetics of the reaction. By increasing the in-cylinder temperature, the oxidation rate also increases during the late cycle. As a result, only a small fraction of the initially formed soot is emitted in the exhaust [38].

Soot only comprises a portion of the total particulate matter. There are two types of particulate matter emitted from typical diesel engines. The first are fractal-like agglomerates of primary particles 15-30 nm in diameter, composed of carbon and traces of metallic ash, and coated with condensed heavier end organic compounds and sulfate. The second are nucleation particles composed of condensed hydrocarbons and sulfate [39]. As regulation on these

particulate matter emissions increases, measurement and characterization of the pollutant have become increasingly complex. Composition measurement of soot is typically preformed outside the engine. A collection substrate is first prepared before sampling the exhaust from the engine via a dilution tunnel. The particulate matter is trapped on the substrate and then can be removed for chemical analysis. By passing a steady flow of diluted exhaust through a filter and recording the mass increase of the filter, the amount of particulate mass can be found. While this records the overall amount of particulate matter mass, it is not enough for chemical analysis [40]. To obtain the full characterization of the particulate matter, it is necessary to use a wide variety of test equipment to measure and characterize the plethora of components. Due to the complexity and cost associated with full characterization, this study is limited to a simple, yet well-developed, filter paper method.

2.5 High Speed Image Processing

High speed imaging is an essential diagnostic tool for understanding combustion phenomenon such as diesel spray injection and combustion. As such, the methods to obtain and process the different aspects of the diesel injection and combustion are important.

2.5.1 Liquid Penetration

Penetration is a spray phenomenon that defines how far a fuel jet travels with respect to time. Several penetration length scales are of interest in diesel injection studies depending on the ambient conditions. These ambient conditions are categorized as non-evaporating conditions, evaporating conditions and burning sprays. Liquid sprays, the liquid penetration, are defined as the distance from the nozzle exit to the farthest location where the liquid phase of the spray

travels. Vaporizing sprays, the vapor penetration, are defined as the distance the vapor portion travels. Burning sprays, the flame penetration, are defined by the distance the tip of the combusting flame travels. Liquid penetration is considered as one of the primary concerns.

The liquid penetration is significantly important because it is one of the decisive parameters in determining the air/fuel mixing ratio. Additionally, it is involved in how the engine or injector is designed as it is a critical design factor to avoid spray wall impingement which potentially can lead to unburnt hydrocarbons and incomplete combustion.

Many different control parameters can affect the liquid penetration to a various degree. Increasing ambient gas temperature will increase vaporization and reduce the liquid penetration. An increase in ambient density will increase entrainment to the fuel. This leads to saturation conditions being met at a shorter distance, thereby decreasing the liquid penetration. Injection pressure barely affects the liquid penetration because the increase of the fueling rate is offset by an increase in the ambient entrainment which is induced by the increase in injection pressure or velocity. As a result it maintains the same fuel-air mixture at an axial location. Since the influence of injection pressure has little effect on liquid penetration, this fact supports the use of elevated injection pressures to improve fuel-air mixing. This assists with emission reductions while avoiding liquid fuel impingement on the cylinder wall to minimize unburnt hydrocarbon emissions.

Naber and Martinez et al. [42, 44] studied spray penetration trends. The spray penetration decreases when the fuel temperature, ambient density, or ambient temperature increases. When the nozzle orifice diameter or fuel boiling point increases, the spray penetration also increases. Increasing injection pressure has no effect on the spray penetration.

Siebers [41] has shown that the liquid penetration trends mentioned above can be explained by assuming mixing-limited vaporization. Siebers used a fuel spray model to calculate the amount of ambient gas entrained into the spray $\dot{m}_a(x)$ relative to the fuel mass flow rate $\dot{m}_f(x)$:

$$\frac{\dot{m}_a(x)}{\dot{m}_f(x)} = \frac{1}{F/A} \propto \frac{x}{x^+} \tag{2.1}$$

$$x^+ = \sqrt{\frac{\rho_f}{\rho_a}} \cdot \frac{\sqrt{C_a} \cdot d}{\alpha \cdot \tan(\frac{\theta}{2})} \tag{2.2}$$

where ρ_a is the ambient gas density, C_a is the orifice area contraction coefficient, d is the injector tip orifice diameter, α is a constant with a value of 0.75 [42], and $\theta/2$ is the jet spreading half-angle.

The fuel ambient ratio $(F/A)_{liq}$ is then calculated by mass where the enthalpy change in the ambient gases matches the energy required to heat and vaporize the liquid fuel at the local liquid-vapor equilibrium temperature. $(F/A)_{liq}$ depends on the ambient gas density and temperature as well as the particular fuel properties and fuel temperature.

$$(F/A)_{liq} = \frac{h_a(T_a, P_a) - h_a(T_a, P_a - P_s)}{h_f(T_f) - h_f(T_f, P_a)} \tag{2.3}$$

where the enthalpy difference in the numerator is the specific enthalpy transferred from the entrained ambient gas to vaporize the fuel. The enthalpy difference in the denominator is the specific enthalpies required to heat and vaporize the liquid fuel.

Using the fuel ambient ratio, the steady liquid penetration (L) can be predicted with this equation:

$$L = \frac{b}{a}\sqrt{\frac{\rho_f}{\rho_a}} \cdot \frac{\sqrt{C_a} \cdot d}{\alpha \cdot \tan(\frac{\theta}{2})} \sqrt{\left(\frac{2}{(F/A)_{liq}} + 1\right)^2 - 1} \tag{2.4}$$

where, *b* and *a* are correlation constants with suggested values of 0.41 and 0.661, respectively.

Liquid penetration length is not only the desired parameter. Spray cone angle is a macroscopic spray characteristic representing the dispersion or spreading of the spray. Dispersion is highly desired as it ensures fast mixing of the liquid and gas phase with a high evaporation rate for optimum combustion. Increased air entrainment which can enhance fuel-air mixing can be obtained as the cone angle increases. Unfortunately, various edge detection techniques are used to measure the cone angle, resulting in different cone angles for the same injector. However, several trends can be uncovered on how the spray cone angle is affected by various ambient conditions [44]. When the ambient density increases, the cone angle also increases. The cone angle decreases with increases in ambient temperature or L/d ratio. Injection pressure and nozzle orifice diameter seem to have no effect on the cone angle.

Various types of diagnosis have been used for diesel fuel injection visualization and characterization including shadowgraphs [42, 43], Schileren imaging [44, 45], and Mie scattering imaging [46-49]. The most commonly used optical method is the shadowgraph. It is an optical method based on capturing shadows cast by the spray. The setup typically requires a light source and a receiver placed on the other side of the spray plume. Therefore this technique is limited to setups with optical access on both sides of the plume. On the other hand, it is a very straightforward technique that requires relatively low sources of light, such as an LED instead of a laser beam. Schileren imaging is more complex, with details found in Ref [45]. The measurement technique also requires optical access on both sides of the spray. The other technique mentioned is Mie scattering. It is done by illuminating the fuel spray with a light

source. The light required is typically stronger and therefore frequently uses laser beams. The light source can be used in two ways: “planar”, like a laser sheet, or “volumetric” such that a scattered laser beam depends on the spray features. For dense spray measurements, planar Mie scattering is not a suitable method for the dense spray measurements. This is because the optical thickness is limited by the laser power and droplets outside of the laser sheet are not captured. In this paper, volumetric Mie scattering was utilized.

2.5.2 Lift-off Length

Diesel sprays are a lifted flame phenomenon. To understand the spatial onset of combustion, the definition of the lift-off length parameter is necessary. The flame lift-off length is defined as the distance between the most upstream locations of the combusting spray in a lifted turbulent diffusion flame to the injector tip [50]. Lift-off length is also influenced by various ambient conditions. When ambient density, ambient temperature, and oxygen decrease, the spray penetration increases. Additionally, the spray penetration trend increases with increasing injection pressure and nozzle orifice diameter [49, 51].

The lift-off length is critical in understanding the combustion and emission formations. The fuel-air mixing upstream of the lift-off length is linked with the resulting soot formation. In general, the increase of the lift-off length leads to a decrease in soot emission. The soot formation is suppressed because of the fact that the average equivalent ratio at the lift-off length is reduced due to the increase of the fuel-air premixing at the upstream of the lift-off length [51].

For the analysis of the combustion and soot measurements, an estimate of the amount of air entrained into a fuel-jet was used. The amount of fuel-air premixing that occurs upstream of the lift-off length will affect the combustion and the soot formation processes downstream of the

lift-off length since the diesel jet is essentially a lifted flame [52]. $\bar{\phi}(x)$ is the cross-sectional averaged equivalence ratio at the lift-off length and is a measure of the amount of air entrained and mixed with the injected fuel upstream of the lift-off length shown here:

$$\bar{\phi}(x) = \frac{2 \cdot (A/F)_{st}}{\sqrt{1 + 16 \cdot \left(\frac{x}{x^+}\right)^2 - 1}} \tag{2.5}$$

where $(A/F)_{st}$ is the stoichiometric air-fuel ratio by mass for a given fuel, x is the axial distance from the injector, and x^+ is a characteristic length scale for the fuel jet defined in Eq. 2.2.

Two sets of conditions can occur when comparing the liquid spray penetration. The first condition is that with a liquid length shorter than the lift-off length. This means that the fuel vaporization is complete before combustion zones are reached. Therefore, there is no interaction between vaporization and combustion processes. The other condition is when the liquid length is longer than the lift-off length, which causes the spray to have a cool-core. This means the vaporized fuel that is surrounded by a rich reaction zone and vaporization cooling can influence the combustion rate, resulting in a reduction in laminar flame speed and an increase in lift-off length [50]. In the case of a shorter liquid length relative to the lift-off length, it is possible that less soot is formed due to a more intense central reaction zone based on the enhanced fuel mixing before the lift-off length [51].

2.5.3 Soot Measurement

Soot reduction is a primary motivation in nearly all diesel-engine related studies. Many new combustion technologies have helped in the reduction of in-cylinder soot emissions in diesel engines. Optical diagnostics provide extremely valuable information on soot formation and oxidation mechanisms as they are non-intrusive, real-time measurements. The optical methods

mainly include planar laser-induced incandescence (PLII) [53, 54], multicolor luminosity techniques [55-57] and laser extinction [58-63].

For PLII methods, a pulsed laser source with duration typically less than 20 ns is used to rapidly heat soot within a laser sheet. The soot is heated from the local ambient soot temperature to the sublimation temperature, or the temperature approximately equal to the soot vaporization, at approximately 4000 to 4500 K. Using collection optics or photodetectors, the incandescence from the soot particles is measured. Information on the soot volume fraction and primary soot particles size are obtained with the appropriate calibration and analysis of the incandescence signal. While PLII provides significant insight into the structure of diesel fuel jets based on the spatial locations of soot, it is limited to qualitative information on soot concentration levels. Optical thickness considerations inhibited attempts to make PLII soot measurements quantitative when standard diesel fuel was used. As a result, PLII measurements for standard diesel fuel are restricted to conditions during the "premixed-burn" phase of diesel combustion when soot levels are low or conditions generated by using low-sooting oxygenated fuels [62].

Multicolor or two-color imaging techniques have also been used to measure soot in diesel fuel jets. The two-color method measures the radiation intensity from incandescent soot particles generated during combustion. Light emitted from soot particles is split into two receiving detectors and then the radiation intensity is measured at the two wavelengths generated by a bifurcation of the light captured. Unfortunately, even though this technique requires additional signal detectors, two-color imaging suffers from high levels of uncertainty [56].

Laser extinction is another technique. While laser extinction is a line-of-sight diagnostic, unlike PLII, it is not limited by optical thickness considerations. Therefore, it can be used to measure soot when standard diesel fuel is used [63]. Conventional laser extinction methods

consist of a light source and a signal detector placed on opposite sides of a soot cloud. More details can be found in Ref [63]. Another soot measurement technique, called forward illumination light extinction (FILE) has been recently developed with the following principles [34]. The FILE measurement consists of a laser beam and camera mounted on the same side of the soot cloud. This is done in the case that there is only one window available for optical access. The scattered laser beam illuminates the region of interest (ROI) and light is reflected back behind the soot cloud by a diffuser mounted on the wall beneath the spray. The reflected light from the diffuser serves as an incident light for the soot measurement. Since it is similar to the conventional laser extinction principle, the ratio of the transmitted and incident light intensity can be related to the optical thickness of the medium using this relationship:

$$I/I_o = e^{(-KL)} \tag{2.6}$$

where K is the dimensional extinction coefficient and L is the path length through the soot. The soot volume fraction f_v can be determined from the dimensional extinction coefficient data using these relationships derived from small particle Mie theory:

$$f_v = \frac{K\lambda}{k_e} = \frac{\lambda}{L \cdot k_e} \ln(I_o/I) \tag{2.7}$$

$$k_e = (1 + \alpha_{sa}) \cdot 6\pi \cdot E(m) \tag{2.8}$$

where λ is the laser wavelength, k_e is the dimensionless optical extinction coefficient, α_{sa} is the scattering-to-adsorption ratio, m is the refractive index of soot, and $E(m)$ is the imaginary part of $(m^2\text{-}1)/(m^2\text{+}2)$ as:

$$E(m) = -Im\left(\frac{m^2 - 1}{m^2 + 2}\right) \tag{2.9}$$

If both the area are represented by each pixel and the soot density are assumed to be known values, with an additional assumption that α_{sa} is negligible, the soot mass at each pixel can be determined as:

$$m_{soot} = f_v L \rho_{soot} A_{pix} = \frac{\lambda}{k_e} \ln(I_o/I) \rho_{soot} A_{pix} \tag{2.10}$$

The soot mass in each frame is obtained and the transient soot mass evolution over one individual injection even can be acquired after image post-processing when all pixel values are spatially integrated over the region of interest.

The FILE method is not perfect as all the uncertainties related to conventional laser extinction measurement also applies to the FILE method. Non-negligible uncertainties exist in the soot optical properties of both *E(m)* and α_{sa} that are required in order to relate the extinction coefficient to the soot volume fraction in Eq. a and b as mentioned in several studies [60].

To date, further research is still necessary to uncover the potential of ABE blends. It can be seen already that ABE improves the emission quality, but the current data sets are rather incomplete. Hence, extensive research is necessary is needed in this area, which is the scope of this thesis. Section 3.1 goes over ABE-diesel combustion tests in a constant volume chamber and section 3.1 goes over the ABE-diesel combustion tests done in a diesel engine. Sections 4.1 and 4.2 go over the results from the constant volume chamber and the diesel engine results, respectively.

Chapter 3

Experimental Facility and Methodology

3.1 Constant Volume Chamber Setup

Despite the abundant discoveries that have been made in engines, the combustion process inside a real engine cylinder is quite complex and its overall behavior controlled is by multiple factors that are highly coupled together. In order to investigate the fundamental nature of the spray at engine-like conditions, constant volume chambers are used to isolate those factors and focus on the thermodynamic processes at a quasi-static flow field. The ABE spray combustion experiments were done in the constant volume chamber.

The experiments were conducted in a pre-burn type constant volume chamber, which is capable of providing high-temperature and high-pressure conditions identical to the conditions upon injection in a real metal diesel engine. Figure 3.1 shows a typical structure of a pre-burn type constant volume chamber.

These pre-burn type constant volume chambers are capable of providing high-temperature and high-pressure conditions similar to typical diesel engine in-cylinder conditions towards TDC (top dead center). The chamber used has a bore of 110 mm and a height of 65 mm, as shown in Figure 3.2. The maximum operating pressure is 18 MPa. The chamber has an open end on the top where a quartz window is placed to allow optical access. The fused silica quartz window, 130 mm in diameter and 60 mm in thickness, is mounted at the top of the chamber and has a high UV transmittance down to 190 nm.

This constant volume chamber has been used by several other authors and additional details can be found in Ref [65, 66, 68, 70, 71, 72, 73].

3.1.1 Injector

The injector used is a 188-1320 Caterpillar HEUI diesel injector. HEUI stands for hydraulically-activated, electronically-controlled, unit injector. Unlike other injectors, it does not rely on high pressure fuel lines and instead relies on highly pressurized crankcase oil. This system allows for higher injection pressures along with accurate injection timing and amount control. The injector specifications are shown in Table 3.1.

The injector is a valve-covered orifice type (VCO), with an orifice diameter of 0.145 mm. The signal input for the current injector is shown in Figure 3.3. The current is pulled up to 7A for 1.8 ms and holds at 4.5 A for 1.7 ms. The total injection duration is fixed as 3.5 ms. Even though the injector signal input changes, the main features of the injector do not change. There is an intensifier inside the HEUI injector with a greater area on the oil side of the plunger than the fuel side. As a result, the pressure exerted on the fuel is magnified with the nominal magnification factor of 6.7.

The HEUI injector has a unique feature of breaking the injection into two separated injections: the "pilot" injection and the "main" injection. It first produces a small pilot injection and a brief delay allows the pilot injection to start burning. From there, the main injection is delivered to the flame front created by the pilot injection. This feature lowers the engine noise by 50 percent.

The injector is mounted on the bottom of the chamber with the injector tip facing upwards. The chamber bottom where the injector is mounted was manufactured to specifically fit the HEUI injector and has fuel and oil lines attached to the injector's corresponding parts. A bracket with O-rings is clamped at the base of the injector where the oil return lines are located. The bracket is attached to a tube, which drains the oil from the injector back into the oil pump.

The hydraulic oil line is filled with SAE 15W-40 oil and pressurized with an oil pump. The oil pressure can be a regulator that controls shop air pressure for the pump. Two bladder accumulators, one placed near the injector and another near the oil pump, are used to maintain pressure during the injection event. It is suggested the maximum oil pressure does not exceed 3000 psi, which corresponds to a peak injection pressure of 138 MPa.

The fuel system consists of a fuel tank and a filter. The fuel tank is pressurized with nitrogen. In order to make sure that particles in the fuel do not damage the injector, the fuel is passed through a filter gauged at 7 microns three times.

3.1.2 Ignition

In order to ignite the premixed combustion, a spark plug and plasma coil are needed. A coil-on-plug system from Ignition Solutions Inc. is installed within the wall with the spark plug electrode protruding from the inside wall. The NGK spark plug is connected with an ignition coil which is attached to a circuit board and wired to a rechargeable 12 V battery controlled by the LabVIEW code. The spark fires when the LabVIEW code sends a 5V TTL signal to the circuit board. The 12 volt battery is connected to a battery charger in order for the battery to retain its charge. The spark can be individually triggered and visually examined in order to make sure that it is operational.

3.1.3 Experimental Preparation

The inside of the chamber is wiped down with acetone soaked disposable towels in order to clean it. Once the surfaces are clear of soot, the chamber is then blasted with compressed air to clear any other debris out. The exhaust port inside the chamber contains eight circular wire

meshes that are replaced every single time the chamber burns fuel. The quartz silicon window surfaces are also cleaned using acetone.

A diffuser is cut out of a sheet of aluminum into a triangle shape that will fit on the bottom surface inside the combustion chamber without interfering with the injector and exhaust ports. The diffuser is placed directly under one injector jet. Adhesive, (Rutland Black: Fiberglass Stove Gasket Cement or Thermeez: 7020 Putty), is applied to the bottom of the diffuser. The diffuser is then placed on the bottom of the combustion chamber, positioning it underneath one of the injector spray jets. The Rutland Black adhesive is given around an hour to dry and then heated gradually with the chamber for a final cure. The Thermeez Putty has to dry for over four hours. If there is insufficient adhesive or the adhesive was not given enough time to cure, the diffuser may fall off or vibrate during the spray combustion event.

High temperature vacuum grease (Dow Corning) is applied to the spring energized seal, until a thin layer of the grease evenly covers the entire surface of the seal. The seal is then placed in the groove carved into the chamber. The quartz silica window is then placed on top of the seal. A paper gasket is placed on top of the quartz window before the metal head is placed on top of it to protect the surfaces from the metal. The metal head is tightened down with four screws to 170 foot-pounds in 15 foot-pound increments using a torque wrench. The seals guarantee that the combustion gases will not leak during the combustion event.

Before spray combustion experiments can be conducted, the chamber walls are heated to mimic the wall temperature of a diesel engine to prevent water condensation on either chamber walls or windows. It also limits the risk of the quartz silicon window cracking from the sudden temperature changes. Eight rod heaters with a total power of 2500 W are inserted into specifically made holes in the chamber body, heating the chamber. In order to control the

temperature of the chamber, a temperature controller with an R-type thermocouple and a 50A Hg Relay are used. The cylinder walls are heated to 378 K before the experiments are started.

A vacuum pump is active throughout the entire experiment for the purposes of evacuating the chamber of its contents when necessary.

3.1.4 Experimental Procedure

Even though the experimental procedure is automatically executed by the Labview program, knowing the actual processes is still important. Figures 3.4 and 3.5 show the layout of all the valves and Table 3.2 shows the valve opening and closing timings. First, the vacuum pump evacuates the Parker ACP hydraulic cylinder, pulling the piston to the back of the cylinder. Each cycle starts with the piston accumulator filling with a premixed, combustible-gas mixture of acetylene (C_2H_2), 50/50 nitrogen and oxygen, and air. The accumulator with the volume of 0.95 liters can provide an ambient density of approximately 15 kg/m^3 inside the chamber upon injection. The concentrations of the different gases in the accumulator will determine the ambient oxygen concentration conditions for the test. The concentrations of the gases are determined by their pressures which can be controlled by the regulators on the gas cylinders.

After the gas finishes filling the accumulator, Valve 6, which is controlled by a step motor, opens. This allows the mixture inside the piston accumulator to be pushed into the vacuumed chamber. The back of piston accumulator is attached to a nitrogen tank and a vacuum line, which pushes and pulls the piston inside. The required pressure for the nitrogen tank is at least 300 psi to ensure sufficient force to push all the gas mixture into the chamber.

The spark ignites the mixture, raising the pressure and temperature inside the chamber. Over the next few seconds (~2 s), the products of combustion cool due to the heat transfer to the

chamber walls and the chamber pressure also reduces. When the desired experimental conditions are reached, the HEUI injector is triggered and the fuel injection, auto-ignition, and combustion processes follow.

Since the fresh pre-burn mixture charge and the exhaust gas after combustion goes in and out of the chamber through the same passage which connects the chamber with the gas line, multiple layers of stainless steel mesh are placed on top of the passage to prevent flam propagation into the gas line. Once the combustion processes finish, Valve 7, which is also controlled by a step motor, opens and the exhaust goes to the main exhaust line through Valve 11. Valve 9 closes and Valve 8 opens so the piston in the accumulator will be vacuumed to the back by the vacuum pressure for the next cycle.

3.1.5 Ambient Condition Controls

Ambient gas temperature, density, and composition at injection are determined by the pressure at the time of fuel injection along with the initial mass and composition of gas within the chamber. Acetylene is used as the combustible gas for its flammability and low window contamination. The chemical reaction equation is shown in Eq. 3.1.

$$4\ C_2H_2 + (10 + \zeta)\ O_2 + 65\ N_2 \rightarrow 8\ CO_2 + 4\ H_2O + \zeta\ O_2 + 65\ N_2 \qquad (3.1)$$

where ζ represents amount of excess oxygen.

The excess oxygen concentration in the products after the premixed combustion can be controlled by the partial pressures of each gas species in the mixture.

3.1.6 Optical Setup

Since the measurements taken on the chamber are all line-of-sight, no laser sheet is needed. High speed imaging is taken using a non-intensified high speed digital camera (Phantom V7.1). The camera was mounted above the optical chamber as shown in Figure 3.6.

Mie scattering was used for the liquid phase detection for the spray studies. Quantitative penetration length analysis were based on the Mie scattering images as Mie scattering predominates when the scattering particles sizes are larger than the incident light wavelength. For the chamber, the fuel droplet diameters were typically in the order of microns and the laser wavelength was in nanometers. Additionally, Rayleigh scattering, which is typically from molecules and tiny particles, is negligible. The method used is a "volumetric" illumination approach rather than a laser sheet. This captures all droplets spreading from the nozzle and to identify the maximum axial and radial distances of any liquid-phase fuel.

The laser used is an Oxford Laser LS20-50 copper vapor laser. It can be externally controlled to run up to a maximum frequency of 50 kHz with pulse duration of 25 ns. The laser has a high external controlled frequency with extremely short pulse duration, which is useful for high speed imaging. A 10-meter fiber is attached to the laser output condenser lens at one end and the other is connected to a condenser lens adapter mounted above the chamber, as shown in Figure 3.6. The emitted laser light from the fiber is condensed by the aspheric condenser lens and the beam direction can be easily adjusted to the desired location. The laser beam has to be tilted with a small angle so the camera's and the laser beam's line-of-sight are not blocked.

The copper-vapor laser has a two-color output, at 511 and 578 nm, with a power ratio of 2:1. Two interference filters were centered at 510 nm and 515 nm respectively, with 10 nm full width at half maximum (FWHM) achieving a 5 nm FWHM. This was to ensure that only the

scattering from the spray is captured and the rest of the spectral range, like the visible soot luminosities > 650 nm, is blocked.

A BNC box was used to synchronize the high speed camera and the copper-vapor laser. The camera is connected to a computer with an Ethernet cable and is controlled with the software "Phantom 663". The camera exposure time is set at 3 microseconds and is not dependent on the image resolution. Different spatial and temporal resolutions were used depending on the parameters of interest. The scattered light from the spray was received by a Nikkor lens with a 105 mm focal lens mounted in front of the camera. The camera is triggered by the injection signal from the LabVIEW code and is set to record several seconds, which is more than enough to cover the entire spray and combustion event. The fine is saved with a ".cine" extension and can be opened with Phantom's Cine Viewer. From there, Matlab can convert the file and further analyze the data.

In addition to the Mie scattering imaging, natural luminosity measurements were done. These tests, however, required that the laser be turned off and different band pass filters are used. For the broadband natural luminosity measurement, all the filters were removed. The luminosity intensity saturation may cause information loss during the combustion analysis, so starting with the minimum aperture for the camera is important to avoiding errors.

Soot measurements were carried out using the FILE technique. The laser and camera setup is the same as the Mie scattering measurements, though in this experiment, an aluminum piece, mentioned earlier, is placed on the bottom of the chamber. The condenser lens adapter is adjusted so that the reflected light from the aluminum piece is as uniform as possible. The aluminum piece will typically become blackened if sooty flames are present and when that

happens, the surface will be dark enough that it could potentially cause errors in the result interpretations.

3.1.7 Data Processing

The in-cylinder pressure is obtained by a pressure transducer. Using the first law of thermodynamics, shown in Eq. 3.2, the apparent heat release rate can be calculated from the pressure trace.

$$\frac{dQ_n}{dt} = \frac{\gamma}{\gamma - 1} p \frac{dV}{dt} + \frac{1}{1-\gamma} V \frac{dp}{dt} = \frac{1}{1-\gamma} V \frac{dp}{dt} \tag{3.2}$$

here γ is the specific heat ratio and Q_n is the apparent heat release rate. Time resolved heat release rate is useful in determining the combustion duration, combustion phasing, and ignition delay. The start of combustion is taken from the curve of the apparent heat release rate. A straight line is fit to the region of the steepest ascent during the rapid rise of the curve. The point where the straight line intersects the time-axis was determined to be the start of heat release. This method is very insensitive to noise and yields an upper limit of heat release start timing. The ignition delay was defined as the difference between the start of heat release and the start of fuel delivery.

The liquid penetration is obtained from pictures taken during the injection event. Raw images from each complete injection sequence are corrected by the first ten images of the sequence which was taken right before the fuel injection to identify the background. From there, histogram equalization was performed to enhance the contrast of each image and minimize the effect of the illumination intensity variation caused by the ambient temperature difference and light degradation. This is done for every sequence of images. This procedure eliminates the bulk noise of the background which makes the determination of both the liquid penetration and

cone angle easier. Before each experiment, a piece of ruler is placed inside the chamber to calibrate the actual pixel length for the camera. Since the camera captures stronger a reflection signal of the laser beam from the spray, the liquid penetration length can be defined as the distance between the injector tip and the threshold pixel along the jet centerline.

The flame lift-off length is determined from the natural luminosity images. Although OH^- is more often used in the lift-off calculation since it is a noticeable mark for the heat release zone, the broadband natural luminosity could provide the general flame structure in a time-resolved manner. The procedures are very similar to that of the liquid penetration calculation, as the injector tip centerline analysis is performed in the same way. The flam lift-off is defined as the distance from the injector tip to the closest pixel above a certain threshold value found in the flame image on the jet centerline.

Optical diagnostics are used in soot measurements since they are non-intrusive and real-time to provide extremely valuable information on the sot formation and oxidation mechanisms. In this case, the soot measurement was done by forward illumination light extinction (FILE). In the FILE method, the laser beam and camera are mounted on the same side of the soot cloud since there is only one window for optical access. The scattered laser beam illuminates the region of interest with a diffuser mounted at the back of the soot cloud. The diffuser reflects the light from the laser and serves as the incident light for the soot measurements. From there, the soot mass at each pixel are spatially integrated over the region of interest and the soot mass in each from is obtained. Afterwards, the transient soot mass evolution over one individual injection event can be acquired after image post-processing.

Baseline measurements are done with diesel to compare with that of the ABE mixtures.

3.2 Engine Setup and Specifications

Data in this study was collected from an AVL 5402 single-cylinder diesel engine. The engine was purchased directly from AVL and all of the associated electronics and software came with the engine. Some of the key engine specifications are shown in Table 3.3. The engine is a basic compression ignition, single-cylinder research engine. The fuel system used is a Bosch CP1 common rail injection system derived from the BMW 3-series and is controlled by an AVL ECU with an ETK7.1 emulator probe. Additionally, the engine uses external support systems for fuel, oil, and coolant.

The engine is coupled to a GE type TLC-15 class 4-35-1700 dynamometer capable of delivering up to 14.9 kW (20 HP) and absorbing up to 26.1 kW (35 HP) at a maximum rotational speed of 4500 RPM. A DyneSystems DYN-LOC IV controller controls the dynamometer. A Kistler type 6125B pressure transducer measures in-cylinder pressure and AVL 3057-AO1 charge amplifier are indexed against a crankshaft position signal from a BEI XH25D shaft encoder.

Figure 3.7 shows a schematic of the engine setup. ETAS INCA was used for the development and calibration of the control and diagnostic parameters in the engine ECM to establish full communication with the engine ECM (AVL RPEMS). Using INCA, data acquisition and real-time recording of many engine operating conditions present in the ECM is possible. An ETAS ES580 interface card is used as the connection between the program and the ECU.

3.2.1 Intake and Exhaust System

Since there is no throttling in diesel engines, the engine is set up to be naturally aspirated. The intake system pulls air through an air filter, which removes the particles in the air, directly from the laboratory. The exhaust from the engine passes through a manifold, a braided flex section and then into the exhaust pipe connected to the building's exhaust. The manifold has several bungs that allows for different measurement devices to be placed. Some of them include a thermocouple for the measurement of exhaust gas temperature in LabVIEW, a NOx sensor, and a sampling port for the emissions analyzer for hydrocarbons and carbon monoxide. When not in use, the bungs are shut so the exhaust gas will not fill the testing chamber.

3.2.2 Oil System

The oil system in the diesel engine uses a mechanically actuated bleed valve which automatically adjusts itself to maintain a system pressure of 60 psi. The system uses SAE 15W/40 or 10W/40 oil and the reservoir can hold around 14 quarts of oil, though 10 quarts is sufficient. The reservoir feeds into a Dayton 6NY34 pump powered by a Dayton 9ND38 0.75 HP motor with the capability of supplying 10.7 gpm of oil at 50 psi. From there, the oil reaches a bleed valve. Since the engine only requires approximately 3 gpm of oil, a bleed valve was added between the oil pump and oil filter, allowing the extra oil to flow back into the oil reservoir. This is so the pump will not be working to force 10.7 gpm of oil into the passages that can only handle 3 gpm. The bleed valve is a simple globe valve so as the oil heats, the pressure will drop and the globe valve must be slowly closed in order to maintain steady oil pressure. The oil that flows through the oil filter enters the engine via stainless steel braided hose. The oil

flows through the engine and then the oil drains from the oil pan of the engine back into the oil reservoir.

3.2.3 Cooling System

The engine uses a blend of 50% ethylene glycol and 50% distilled water in a ratio of 1:1. The engine does not have a thermostat or an internal water pump so all of the cooling system components are separate from the engine. The total cooling capacity of the system is approximately 8 L. A Young Radiator Company liquid-liquid heat exchanger model F-302-EY-1P is the main component of the cooling system. Both engine coolant and water from the building flow through the heat exchanger. The building's water carries the heat away from the coolant. A Moroso 63650 1.5L aluminum expansion tank with a maximum pressure limit of 1 bar is used to add coolant to the system. The expansion tank is piped directly into the heat exchanger.

The water from the building is applied to the cold side of the heat exchanger where the engine coolant is exiting the heat exchanger. The water travels through the heat exchanger and into the building drain. A shut-off valve is installed upstream of the heat exchanger to stop the flow of water when the engine is not running.

After the engine coolant flows through the heat exchanger, it enters a Dayton 4RU72 centrifugal pump. From the pump, the coolant flows through a gate valve used to throttle the coolant flow and into an Ashcroft safety switch. The switch (model number FS5-3/4) can shut down the engine when the coolant is not flowing. The coolant then flows into the engine via a braided copper flex tubing and exits the engine on the front intake side of the engine head. The hot coolant flows into a Sterlco thermostatic valve (part number R-151-F) which regulates the

coolant flow based on the temperature of the hot coolant. The cycle then repeats as the coolant flows into the heat exchanger.

3.2.4 Fuel System

The fuel system for the diesel engine consists of two very different yet interconnecting fuel systems. This includes the low pressure fuel system and the high pressure fuel system. It is important that the fuel inside of the fuel cell is completely filled at all times when the engine is running. This is because if the fuel cell is low, the high pressure pump could run dry and become damaged as the fuel is used to lubricate the pump.

A schematic of the low pressure fuel system is shown in Figure 3.8. The low pressure fuel system supplies the fuel from the fuel tank to the high pressure system. The fuel is stored in a five gallon RJS Racing Equipment fuel cell (model no. 10992). The fuel flows from the fuel cell into a 12 V low pressure fuel pump under the force of gravity. From there, the fuel is pressurized and passes through a CAT fuel filter (P/N 1R-0751). The fuel pressure can be observed just after the filter since a pressure gauge is placed there. The fuel is then air cooled with forced air convection by a tube and fin air-liquid cooler and a Spal Type VA21-A37/C-45A 12 V electric fan. The cooled fuel travels through copper piping to the high pressure fuel pump.

The high pressure fuel pump was supplied by AVL for the engine used. The fuel from the low pressure system is pressurized to between 400-800 bar by the high pressure pump. A measuring unit attached to the pump maintains a certain fuel flow for the high pressure pump and is pre-controlled by the fuel pressure controller. From there the fuel enters the fuel rail. A fuel pressure sensor is connected to the ECU in order to acquire and control the fuel rail pressure in the high pressure rail. The fuel then is either injected into the engine or flows out of the pressure

control valve. The pressure control valve is a control element for the rail pressure controller. If the fuel pressure is too low, the valve will close. If the pressure is too high, the valve is opened by the ECU.

Once the fuel has traveled through the high pressure fuel system, the fuel that did not enter the engine will flow into the fuel distribution block. From there, the fuel distribution block transfers the fuel into the low pressure system and back into the fuel tank.

3.2.5 Emission Analysis

In-cylinder pressure traces shown are the average of 25 combustion cycle pressure traces. A Horiba MEXA-720 NO_x non-sampling type meter in the exhaust manifold of the engine measures the NO_x, λ and Φ. The range of measurement for NO_x is 0-3000 ppm with ±30 ppm accuracy for 0-1000 ppm, ±3% accuracy for 1000-2000 ppm, and ±5% accuracy for 2000-3000 ppm. A Horiba MEXA-554JU sampling type meter was used to take measurements of unburned hydrocarbons (UHC) and carbon monoxide. A probe was fabricated to fit in the exhaust manifold of the engine which allowed the sampling tube to transport the exhaust gases to the meter. The measurement range is 0-10,000 ppm for unburned hydrocarbons, 0.00-20.00% by volume for carbon dioxide, and 0.00-10.00% by volume for carbon monoxide. A type-K thermocouple located in the exhaust manifold was used to measure exhaust gas temperature.

Soot measurements were performed using a standard filter paper method. Samples of raw exhaust gas are drawn through a 7/8” round filter paper using a vacuum pump. Rectangular strips of filter paper supplied by Grainger Industrial Supply (#6T167) were cut into discs and placed in a filter holder taken from a Bacharach True-Spot smoke meter, which was adapted to the new setup. A line filter installed after the vacuum pump to remove condensed water or oil.

After sample collection, a digital scanner was used to measure the filter blackening. The paper blackening (PB) is defined as:

$$PB = (100 - R_R)/10 \tag{3.3}$$

$$R_R = \left(\frac{R_p}{R_f}\right) \times 100\ \% \tag{3.4}$$

where R_p is the reflectometer value of sample, R_f is the reflectometer value of unblackened paper, and R_R is the relative brightness of the sample (relative radiance factor).

A flow meter controlled by a needle valve on the inlet of the vacuum pump is used to monitor the sampling flow rate. In order to achieve an effective sampling length of 405 mm, the flow rate and sampling duration is selected based on the expected soot content. With the sampled volume at 1 bar and 298 K, the paper blackening value can be considered as the filter smoke number (FSN). More details can be found in Ref [74].

Measurements of UHC, CO and exhaust gas temperature (EGT) measurements were recorded directly from the emissions analyzer while measurements of brake toque, lambda, and NO_x were averaged of a 60-second period. In-cylinder pressure traces were taken for all fuels to examine the combustion characteristics. Experiments were performed three times and the datasets collected were then averaged. The effects of humidity were assumed to negligible as the tests were performed in a temperature-controlled laboratory. The engine was allowed to run at every operating condition for an extended period of time to ensure steady state measurements.

3.2.6 Test Fuels

The fuels tested in these experiments were D100, ABE10, and ABE20. The acetone-butanol-ethanol (ABE) used in this experiments were vol.% of acetone, butanol and ethanol were kept at 30%, 60% and 10% respectively. D100 stands for 100% pure diesel. ABE10 stands for

10% acetone-butanol-ethanol mixture and 90% diesel by volume. ABE20 consists of 20% ABE and 80% diesel by volume. The physical and thermo-physical properties of each component in the mixture are listed in Table 2.1.

3.2.7 Test Conditions

In this study, a 5-condition test matrix was adopted to run the engine at three different speeds (1200rpm, 1500rpm and 2000rpm) with constant load of 20mg fuel injected per cycle, in order to achieve a speed sweep; the load sweep is performed at the constant speed of 1200rpm, with 15mg, 20mg and 25mg fuel injected per cycle. Four different injection timings are tested under each condition in order to study the timing dependence of engine performance and emissions. The test conditions are summarized in Table 3.4.

Chapter 4

Experimental Results and Discussion

4.1 Constant Volume Chamber Results

4.1.1 Impact of Acetone

In Ref. [65, 66], the impact of acetone contents in ABE mixtures when blended with diesel under the ratio of 20% (in terms of ABE, volumetric) were investigated. In this work, three different compositions were tested: ABE (3:6:1), ABE (6:3:1) and ABE (0:10:0). Although it is hard to isolate the acetone content influence from the mixture compositions tested, some qualitative conclusions can still be made.

Figure 4.1 shows the pressure trace and apparent heat release rate of the spray combustion. A direct implication can be made from all three figures that ABE20(6:3:1) has the most similar combustion characteristics as that of pure diesel, resulting in the similar shape and peak value of both pressure trace and AHRR. Compared to ABE20(6:3:1), both ABE20(3:6:1) and ABE20(0:10:0) showed retarded combustion phasing and also showed relatively milder combustion. Despite the fact that the two fuels are quite distinct in butanol concentrations, ABE20(3:6:1) and ABE20(0:10:0) have a closer AHRR curve than they appear with ABE20(6:3:1). In this case, it can be concluded that acetone has a major effect of advancing combustion phasing, which can be attributed to the high volatility of acetone. Also, the chemical nature of acetone during combustion, with a higher laminar flame speed (Table 2.1) will result in an accelerated combustion for ABE20(6:3:1).

In terms of cleanliness of the combustion, spatial integrated natural-flame luminosity (SINL) was proposed as a factor to describe the time-resolved overall soot emission during combustion. As stated by Dec et al. [67], the natural flame luminosity is essentially an indicator

of soot concentration and soot temperature. Figure 4.2 shows the evolution of SINL during the combustion process for each fuel tested. It can be seen that the soot emission is highly related to the ambient oxygen concentration: with a decreased ambient oxygen concentration from 21% to 16%, more than 50% decrease in SINL peak value can be observed, the results in ambient oxygen of 11% were not shown, because the camera was not able to capture the flame luminosity signal with the same aperture setup. However, compared to ABE20(3:6:1) and ABE20(0:10:0), the SINL of ABE20(6:3:1) is usually higher. This may be attributed to the insufficient premixing process prior to combustion, due to the advanced combustion phasing. It is believed that an optimized acetone concentration can both ensure the proximity of combustion behavior as pure diesel, but will also decrease the soot emission to the desired extent.

4.1.2 Impact of Butanol

In order to investigate the impact of butanol content in ABE mixtures, neat ABE (referred to as ABE100) with a volumetric ratio of A:B:E=3:6:1 and neat n-butanol (referred to as B100) were studied [68]. Additionally, pure diesel (referred to as D100) was compared to as a baseline. Figure 4.3 shows the liquid penetration length measured with high-speed Mie-scattering images captured in experiment. The liquid penetration lengths of ABE100 and B100 are shorter than that of pure diesel, but they themselves showed little difference, except for low ambient temperature conditions (800K). This is mainly because of the volatility of acetone, butanol and ethanol: at lower temperatures, the effect due to the difference in volatility is amplified: ABE100 with the more volatile acetone and ethanol contents shows better evaporation and mixing prior to combustion.

In terms of combustion characteristics, Figure 4.4 shows the pressure trace and apparent heat release rate of tested fuels under different temperature conditions. At higher temperature,

ABE100 and B100 show similar combustion phasing and AHRR shape. However as the ambient temperature decreases, the deviation between these two fuels starts to become evident, as ABE100 generally showed retarded combustion phasing and even lower peak AHRR than B100. This characteristic is similar with the observation in liquid penetration lengths, because the evaporation process is a major factor that controls the initial stage heat release pattern: with a shorter penetration length, better liquid fuel atomization and evaporation can be expected and thus leading to a more rapid pressure rise, in this way, spray penetration length can be correlated to the heat release rate, which is consistent with the observation in this research.

The proximity of modifying the ABE mixture in both evaporation and combustion ABE100 and n-B100 characteristics in terms of both spray and combustion also revealed that butanol as the most redundant species in ABE mixture, has the effect of controlling overall spray and combustion characteristics. In the application of ABE fuel, certain amount of butanol in ABE mixture is desired for the following purposes: (1) Increase energy density of the mixture; (2) Adjust the overall volatility of mixture to an appropriate level; (3) Counteract the retardation effect of acetone and ethanol to an appropriate level.

Apart from these merits, as observed in Ref [68], higher butanol content may cause an increment in soot emission. Figure 4.5 shows the spatial integrated natural flame luminosity (SINL) of pure diesel, ABE and n-butanol during constant volume combustion, which adds up pixel-by-pixel natural flame luminosity to evaluate the overall luminosity emission during combustion. The natural luminosity results from two sources: chemiluminescence and soot incandescence. However, in general combustion cases, the intensity of soot incandescence, which depends on local soot concentration and soot particle temperature [67], is much stronger than the former one [69]. In this way, it can be expected that SINL is an indicator for overall

combustion cleanliness. As is shown in Figure 4.5, The SINL curve of B100 has a higher peak than that of ABE100. However, the reduction in soot concentration of both ABE100 and B100 compared to pure diesel is already quite satisfactory.

4.1.3 Impact of Ethanol

As been stated before, ethanol is usually a minor amount (~10% vol.) in the current fermentation process of ABE mixture. As a result, the investigation concerning the impact of ethanol content in ABE combustion is very rare. However, through comparing the previous results of different ABE compositions and pure butanol (Figs. 4.1 and 4.4), it can be seen that ethanol content has a retardation effect to the ignition timing of the mixtures. Note that ethanol is usually a minor species in the tested fuels. This retardation effect can be quite strong, and can be attributed to the lower cetane number of ethanol, when compared to both butanol and diesel.

4.1.4 Impact of ABE-Diesel Blends

As a convention in the market, biofuels or alcohols are usually blended with commercial transportation fuels at a certain ratio. In order to study the impact of ABE-diesel blending ratios, a lot of work has been done. In this part, several works on spray and combustion characteristics of different ABE-diesel blends will be summarized.

The combustion characteristics of ABE20 were analyzed at various temperature and ambient oxygen concentration conditions [70]. High-percentage ABE-diesel blend (ABE80) were further focused on in Ref [72]. Data from all these papers are gathered to offer a better representation of blending ratio influences.

In terms of liquid penetration length, with the addition of ABE in diesel, a shortened liquid penetration length will be observed. Also, similar to previous results, as the ambient

temperature decreases, the deviation between fuels will start to stand out more obviously, owing to the difference in volatility of ABE and diesel.

In terms of combustion characteristics, Figure 4.6 shows the combustion pressure and AHRR curves for the tested fuels. Note that the lines are not spreading with the same sequence of increased ABE content: ABE50, although contains more ABE, appear to be more advanced in the combustion phasing than ABE20. This observation indicates that there are at least two competing factors that are influencing combustion characteristics at the same time. Some obvious factors include the low cetane number and the high latent heat value of ABE, which will both lead to a retarded auto-ignition timing. Other reasons that will lead to advanced combustion timing could be a better fuel-air mixing prior to combustion, as the high oxygen content improves the local air-fuel ratio. Due to this competing process, ABE20 suffers from higher latent heat and lower cetane number resulted by ABE. But this is not compensated through enhanced evaporation and fuel-air mixing, which leads to an overall retarded combustion phasing. ABE50 seems to be the best ratio among the tested fuels, for its proximity in combustion characteristics with diesel and thus providing a potential to be directly used in an engine without the need of modification. It can also be inferred that there should be an optimal ABE-diesel blending ratio, to better balance these competing factors.

In terms of soot emission during combustion, SINL evolution histories of tested fuels under different ambient oxygen concentrations and ambient temperature conditions are presented in Figure 4.7. Some general conclusions concerning low soot emissions during low temperatures and low ambient oxygen concentrations can be easily made, indicating that LTC and EGR are still effective soot controlling strategies of the ABE-diesel mixture combustion.

A proportional relation between ABE concentrations in diesel blend and maximum SINL value can be observed under all conditions. Also, note that the width of SINL plateau is decreased with the increased ABE ratio. These findings are both attributed to the oxygen content in ABE mixtures. On one hand, oxygen content will improve the local equivalence ratio during the non-premixed combustion process, which can significantly decrease the generation of soot precursors. On another hand, the overall lean-mixture due to the oxygen-content in fuels will accelerate the soot oxidation process, resulting in a shortened soot presence time.

4.2 Engine Results

In this section, experimental results concerning the engine performance, combustion characterization and engine-out pollutant emissions are analyzed and presented. The scope of this section is to provide a comparison between three fuels with increasing ABE content and to explore the potential of using ABE to improve engine performance.

4.2.1 Engine Performance

An overall evaluation of engine performance under all test conditions is presented in the following section. Note that due to the higher heat of vaporization (HoV) of the ABE species and the resulting charge cooling effect, some of the conditions that were fueled with ABE-containing diesel mixtures misfired and no positive engine power outputs were achieved. This phenomenon is more severe at retarded injection timing (4^{o}CA ATDC). Thus, the contents discussed below are limited only to the cases with injection timings prior or equal to TDC (8^{o}CA BTDC, 4^{o}CA BTDC, 0^{o}CA BTDC). Table 4.1 summarizes the valid conditions of tested fuels.

Figure 4.8 shows the indicated thermal efficiency (ITE) under aforementioned valid test conditions of all tested fuels. The ITE curves are separated into groups of different ABE content: an increasing ABE content in diesel mixtures will result in a higher ITE almost for all

cases. It should be noted that with only 10%vol. ABE blended in diesel, the ITE increases significantly by roughly 4-6 percentage points. Further addition of ABE (ABE20) in diesel results in a relatively slight increase of ITE, compared to that with ABE10. This improvement can be attributed to the high volatility of fuel additives that enhanced vaporization and fuel/ air mixture preparation processes. The fuel-borne oxygen in the ABE species is also a potential factor to consider, as it enhances the oxidation processes of incomplete combustion products. This is consistent with results in the previous research: Chang et al. [31, 32] observed similar improvement on efficiency in a diesel-powered generator by blending 20% vol. ABE with diesel.

Figure 4.9 shows the power output of the engine fueled with pure diesel, ABE10 and ABE20. The data from the medium load condition (20mg/ stroke) and the injection timing of 8^{o}CA BTDC are presented. Engine performances at other tested conditions show a similar trend as shown in this figure. It can be seen that with ABE addition, engine power output decreased slightly to 5% of the maximum.

Based on previous studies concerning alcohol fuel additive effects, it is expected that engine power output will be decreased due to their reduced lower heating values (LHV) [24]. However, it can be seen that engine power output of ABE-diesel mixtures is almost identical with that of pure diesel. This means that the degradation of the overall energy content that ABE brought about had been fully leveraged and recovered by the higher combustion efficiency.

In conclusion, the addition of ABE into diesel improved the indicated thermal efficiency and at the same time maintained a similar level of engine power output. In the following section, the combustion and heat release patterns will be analyzed to further validate and interpret the efficiency improvements.

4.2.2 Combustion Characteristics

The details of the engine combustion processes can be obtained by analyzing heat release rate curves, which can be obtained from in-cylinder pressure traces. The calculation assumes thermodynamic equilibrium during combustion in the cylinder, which can be expressed via Equation 4.1:

$$\frac{dQ}{dt} = \frac{\gamma}{\gamma - 1} p \frac{dV}{dt} + \frac{1}{\gamma - 1} V \frac{dp}{dt} \tag{4.1}$$

where, γ is the ratio of specific heats. It is considered as a constant in the calculation of this study.

In this section, the traces shown are the mean traces of several 25 consecutive engine cycle samples recorded over a 60 second period and used to calculate the heat release rate (HRR). Then the cumulative heat release (CHR) was calculated by integrating HRR over crank angle degrees and normalized by total heat released. A temporal bandpass filter was applied to the HRR in order to eliminate noise by the end of combustion and the induced overestimation of combustion duration. Based on the CHR curves, the ignition delay is defined as the time between injection and 10% cumulative heat release, the combustion duration is defined as the time between 10% and 90% cumulative heat releases.

4.2.3 Pressure Trace and Heat Release Rate

Figure 4.10 shows pressure trace and heat release rate at three different injection timings at 1500rpm for the tested fuels with injection quantity of 20mg per stroke. It can be seen that with the addition of ABE, the peak combustion pressure and maximum heat release rate is higher than that of pure diesel, except for the case of late injection at 0^{o}CA BTDC. The reason for this exception is mainly due to the ignition delay. It is clear from the HRR curves that ABE10 and

ABE20 have significantly prolonged ignition timing compared to the other two injection timing cases. The start of combustion is progressively retarded with ABE addition and extends into the expansion stroke. Higher combustion pressure can relate to higher combustion temperature, which might favor the production of NO_x. Emission measurement results will be discussed in the following section in more detail. It should also be noticed that the timing of peak combustion pressure retarded with the addition of ABE contents. This effect is almost linearly proportional to the ABE content. In a well-tuned engine, peak pressure timing should be around 10~15^{o}CA ATDC [9]. The retardation effect indicates that when replacing pure diesel with ABE-diesel mixtures, the injection timing needs to be adjusted to be more advanced.

The heat release rate curves are almost identical in shape for the tested fuels. However, ABE-containing fuels usually have a higher HRR peak at the injection timing of 8 and 4^{o}CA BTDC. The reason for this is the longer ignition delay time, and combined with the high volatility of ABE species, allows for more fuel to be vaporized before combustion and results in a more premixed- dominant combustion. Usually, a higher peak HRR is an indicator of higher thermal efficiency [75], which is consistent with the measured ITE results shown in the previous section.

4.2.4 Combustion Phasing

The quantified parameters to be discussed in this section are extracted from the abovementioned CHR curve. These parameters include: ignition delay, which is defined as the time between injection and 10% cumulative heat release; CA50, which is the timing of 50% cumulative heat release; combustion duration, which is defined as the time between 10% and 90% cumulative heat release. Figure 4.11 and Figure 4.12 show the combustion characteristics under a timing sweep and a load sweep, respectively. In each figure, the gray columns, which

start from the injection timings, represent the ignition delay. The orange columns indicate the timing spans of the first half of combustion, during which premixed combustion is the dominant mode. The blue columns indicate later halves of combustion. The red lines between blue and orange bars are the indicator of CA50 location. Values in white color at the bottom of each bars are the ignition delay time, ones in black color and located at the top are the combustion duration time.

From both figures, it can be seen that the ignition delay time increased with more ABE content. This is mainly due to the charge cooling effect and the low cetane number of the ABE species. Both these factors prolong the ignition delay period. This observation is consistent with previous research with both the constant volume chamber and SI engine results [27]. Generally, the outcome of longer ignition delay time is that it allows for more liquid phase fuel to be vaporized during this period and thus resulting in a more premixed-dominant and more rapid combustion reaction rate at the first stage. The orange bars, representing CA10~CA50 time spans, further proves this implication: it can be seen that the length of this period shortened with the addition of ABE content, meaning a faster heat release. As with the timing of CA50, it can be seen from both figures that, with increasing ABE concentration, the occurrence of CA50 will be slightly retarded, similar to the results seen in peak cylinder pressure comparison. Since the changes in CA 50 are minor, it can be argued that the necessity for changes in the ECU maps is unneeded when using diesel blended with up to 20% ABE. However, in the case of optimization, the ECU maps should be adjusted. Lastly, combustion duration was approximately linearly decreasing with the addition of ABE content, which is consistent throughout all cases presented in Figures 5 and 6. The main reason for this observation may be attributed to the combination of

higher degree of premixed combustion (CA10~50) and higher reactivity during diffusion combustion period (CA50~90).

Figure 4.11 shows the combustion phasing of the tested fuels at different injection timings. There is an obvious trend that for all tested fuels, retarding injection timing will shorten the combustion duration, while ignition delay stays almost the same (for the 8^{o} CA and 4^{o} CA BTDC cases). This can be attributed to the increased degree of incomplete combustion at retarded injection timing, which is consistent with the results of ITE and further observations in soot emissions.

Figure 4.12 shows the combustion phasing diagram in regards to the injection quantity per cycle. The observations again confirmed that ignition delay would increase with the increasing amount of ABE in diesel. Apart from this, another observation concerning injection quantity is that by increasing injection quantity, combustion duration will become longer while the ignition delay will become shorter. The explanation for the shortened ignition delay time is that there are several competing factors that have an effect on the ambient temperature before combustion: charge cooling effect can reduce ambient temperature, cooling water temperature may also change due to the different load conditions. Although cooling water temperature was kept as a constant in this study, transient change in temperature is inevitable especially in the high load conditions. In this case, the shortened ignition delay time at larger injection quantity can be attributed to the higher transient engine temperature, while the charge cooling effect played as a minor role.

As a conclusion to this section, ABE-containing fuels have the combustion characteristic of longer ignition delay time, shorter combustion duration and higher rate of combustion during

the premixed combustion process. Although rate of combustion is faster, the overall timing of ABE-containing fuels are slightly retarded, in regards to CA50 and end of combustion.

4.2.5 Pollutant Emissions

Figure 4.13 shows the trade-off relations between NO_x and PM emissions for pure diesel, ABE10 and ABE20, under various engine speed conditions. For clearer presentation, only data from injection timing of 8^o CA BTDC is showed.

Generally, for all three fuels tested, NO_x emissions increased while PM emissions decreased. This is a widely accepted phenomenon in diesel engine combustion. As for the emissions compared between different fuels, it can be seen that with the addition of ABE, a relatively higher NO_x emission and a lower PM emission were observed. This is mainly due to the higher in-cylinder peak pressure, i.e. higher combustion temperature, which promoted NO_x generation in thermal-NO pathway. At the same time, a premixed-dominated combustion will suppress soot generation processes as it reduces fuel-rich areas. In addition, higher combustion temperature will favor the soot oxidation process by enhancing the oxidation reaction rates. These factors are basically results of the higher volatility of ABE mixtures compared to pure diesel.

When further examining the data shown above, it can be seen that the changes in emissions are not linearly proportional to the ABE content in mixtures. Take the PM emissions for example: at 2000rpm, when adding 10% ABE to diesel, FSN values decreased by a factor of 34%. When further increase ABE content by another 10%, FSN value decreased only by a factor of 13%. At some load conditions, the emission of ABE10 and ABE20 mixtures even showed a similar emission level. This observation further suggested that even when blending ABE by a

minor concentration as low as 10%, it would have a significant effect on combustion and emission characteristics of the mixture.

Although Figure 4.13 suggests that the addition of ABE will result in an increased level of NOx emission, Figure 4.14 presents another way of looking into this issue. In Figure 4.13, the emission data is compared at the same load condition and injection timing, which correspond to the situation of using ABE-diesel without changing engine ECU calibration. Figure 4.14 shows the emission characteristics over the injection timing sweep. The lower group of lines representing FSN comparisons again confirms the fact that increasing ABE content will be helpful for the reduction in soot emissions. The upper group of lines shows that for all three tested fuels, NO_x emissions decreases with retarded injection timing. However, the rate of decrement varies. At the injection timing of 8^oCA BTDC, pure diesel has the lowest NO_x emissions. As injection timing is retarded, ABE10 and ABE20 gradually prevail and have drastically lowered NO_x emissions compared to pure diesel.

As a brief conclusion to the above observations, ABE-diesel mixtures have the potential of decreasing soot emission and NO_x emission at the same time. It should be noted that when using ABE-containing fuel, engine ECU needs to be optimized for high efficiency and low emissions.

Chapter 5

Conclusions and Future Work

This paper summarized the issues concerning a new biofuel: acetone-butanol-ethanol (ABE) when blended with diesel, while focusing on a more fundamental approach to investigate the spray and combustion process in a quasi-static flow conditions. Some main conclusions include:

- Acetone is the major species in the ABE mixture that influences the combustion phasing. Increasing acetone content will result in a significantly advanced combustion phasing. Too much acetone content can lead to an increase in soot emission during combustion.
- Butanol has a minor effect on ignition delay time, but it is a crucial component for the ABE mixture, acting as a "mediating" species to compensate the degree of combustion phasing advancement caused by acetone and ethanol. Also, butanol has the highest heating value, which is important for the increase of overall fuel energy density.
- Blending the ABE mixture with diesel has a proportional effect of decreasing soot emission and accelerating soot oxidation. However, the combustion characteristic of the ABE-diesel mixture is dominant by several competing factors. An optimal ratio of ABE in diesel exists near 50% which will produce a similar behavior as pure diesel.

Based on the review, several undermining yet important topics of ABE research are needed:

- Validate the minor effect of ethanol in ABE-diesel mixture, in terms of both combustion characteristics and pollutant emissions.
- Construct guidelines for optimizing ABE-diesel blending ratios, including the identification of competing factors and numerically modelling of optimization problems.

- Validate the results using experimental results of ABE-diesel fueled diesel engines.

However, several challenges are faced in this area of research, which need to be considered for the future work.

- Due to the composition of ABE mixture, single-factorial design of experiment is not possible: changing concentration of one component will surely affect the other two. This issue makes the conclusions unconvincing, and obstructs the quantitative analysis of the problem.
- Incomplete reaction during premixed combustion of constant volume chamber can be expected. However, the minor species during this incomplete combustion process could act as precursors or introduce radicals for the following spray combustion process. Analysis of the degree of reaction and species after premixed combustion is important.

The performance and emission of a compression ignition engine fueled with ABE/diesel mixture were investigated. The results showed a promising future for ABE-diesel mixture as an alternative transportation fuel. Some key features of ABE-diesel mixture combustion are as follows:

- Improved thermal efficiency even with a relatively small ABE blending ratio.
- Slight reduction in power output due to lower energy density.
- Overall retarded combustion phasing, including longer ignition delay time, retarded CA50 timing and peak pressure timing together with end of combustion timing.
- Accelerated heat release during CA10~CA50, indicating a higher degree of premixed combustion.

- Soot emissions will be lower, NO_x emissions will be higher for ABE-containing fuels at same load and timing conditions.
- Tuning injection timing is helpful for the reduction of NO_x to a degree that is even lower than that of diesel.

In general, by proper tuning of injection quantity and injection timing in engine, adopting ABE-diesel mixture has the potential of improving efficiency and reducing emissions at the same time without sacrificing engine performance. Considering the low cost of ABE production compared to other kinds of bio-fuels, ABE could become a possible substitution to the current fuel additives.

Tables

TABLE 2.1: Physical and thermodynamic properties of ABE-diesel blends and their pure components.

Properties	***Diesel***	***Acetone***	***Butanol***	***Ethanol***	***ABE20 (6:3:1)***	***ABE20 (3:6:1)***	***ABE20 (0:10:0)***
Molecular formula	C_{12}–C_{25}	C_3H_6O	C_4H_9OH	C_2H_5OH			
Cetane number	>40		25	8			
Oxygen content (wt %)		27.59	21.62	34.78	5.08	4.77	4.21
Density at 288 K (g/mL)	0.82-0.86	0.791	0.813	0.795	0.832	0.833	0.835
Auto-ignition temperature (K)	503	833	658	707			
Lower heating value (MJ/kg)	42.7	29.6	33.1	26.8	40.34	40.53	40.83
Boiling point (K)	555-561	329.2	390.8	351.5			
Stoichiometric ratio	14.3	9.54	11.21	9.02	13.47	13.57	13.7
Latent heat at 298 K (kJ/kg)	270	518	582	904	328.7	332.8	330.8
Flammability limits (vol. %)	0.6-5.6	2.6-12.8	1.4-11.2	4.3-19			
Saturation pressure at 311 K (kPa)	0.3	53.4	2.27	13.8			
Viscosity at 413 K (mm^2/s)	1.9-4.1	0.35	2.63	1.08			
Laminar Flame Speed (cm/s)		~34[a]	~48[b]	~39[c]			

Note: (1) Properties of diesel are from ASTM D975, properties of acetone are from [10, 11], properties of ethanol and butanol are from [10-12]. (2) Laminar flame speed data from [13], under conditions: a- 1atm, 298K; b- 1atm, 343K, c- 1atm, 325K.

TABLE 3.1: Injector parameters.

Nozzle type	Valve-covered orifice
Number of nozzle holes	6
Orifice diameter	0.145 mm
Injection duration	3.5 ms
Fuel Temperature	350 K

TABLE 3.2: Valve timings from Ref. [73].

	Vacuum	Fill				Image	Discharge
		C_2H_2	Air	N_2	Chamber		
V1	×	√	×	×	×	×	×
V2	×	×	×	√	×	×	×
V3	×	×	√	×	×	×	√
V4	×	×	×	×	×	√	×
V5*	√	√	√	√	×	√	√
V6	×	×	×	×	√	×	√
V7	×	×	×	√	×	×	√
V8	×	×	×	×	×	√	√ | ×
V9	×	×	×	×	√	×	×
V10	×	√	√	×	×	×	×
V11*	√	×	×	√	√	√	√

* These two valves are normal open while all the other valves are normal close

√ Valve opens

× Valve closes

TABLE 3.3: Engine specifications.

Engine	AVL 5402 Diesel engine
Number of cylinders	1
Bore	85 mm
Stroke	90 mm
Displaced volume	510.7 cm^3
Number of valves	4
Compression ratio	17.1:1
Diesel injection	Direct injection
Diesel Injection system	BOSCH common rail CP3
Number of injection holes	5
Diameter of injection holes	0.18 mm

TABLE 3.4: Engine test conditions.

Engine Speed [rpm]	1200, 1500, 2000
Load [mg fuel/cycle]	15, 20, 25
Injection Timing [^{o}CA BTDC]	8, 4, 0, -4
Fuel Rail Pressure [bar]	600

TABLE 4.1: Condition validity at retarded injection timing (4°CA ATDC).

Load (mg fuel/ injection)		15	20	25
D100	1200rpm	Valid	Valid	Valid
	1500rpm		Valid	
	2000rpm		Misfire	
ABE10	1200rpm	Misfire	Misfire	Valid
	1500rpm		Misfire	
	2000rpm		Misfire	
ABE20	1200rpm	Misfire	Misfire	Misfire
	1500rpm		Misfire	
	2000rpm		Misfire	

Note: Grayed unit stands for conditions not included in the experiment matrix.

Figures

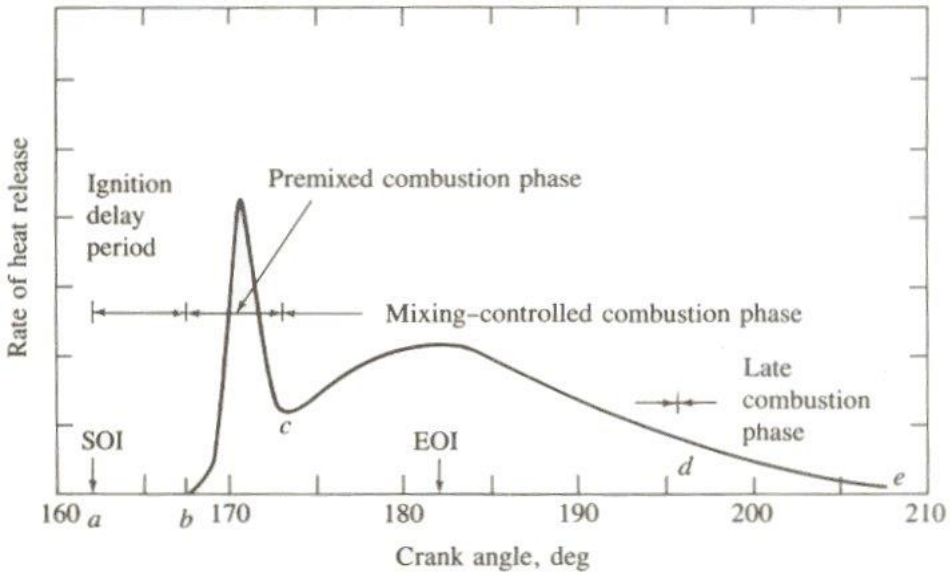

FIGURE 2.1: Typical heat release rate diagram for a direct injection diesel engine [9].

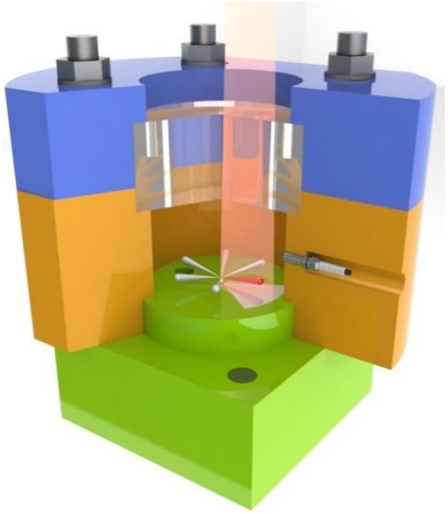

FIGURE 3.1: Inner structure of a pre-burn type CVC, experiment setup as shown in Ref. [18].

FIGURE 3.2: Constant Volume Chamber from Ref. [73].

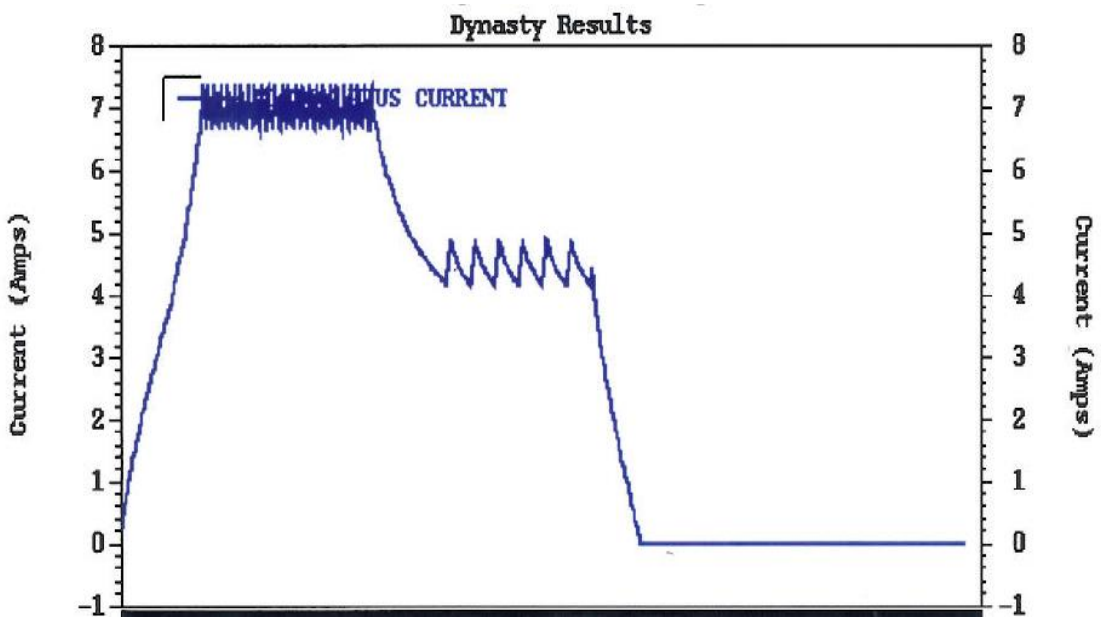

FIGURE 3.3: Current signal of HEUI injector from Ref. [73].

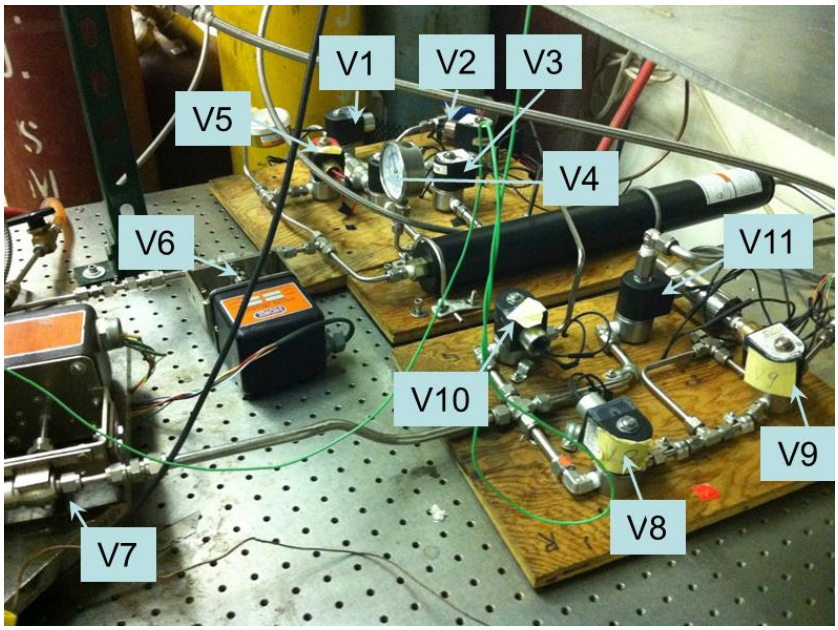

FIGURE 3.4: Valve arrangement from Ref. [73].

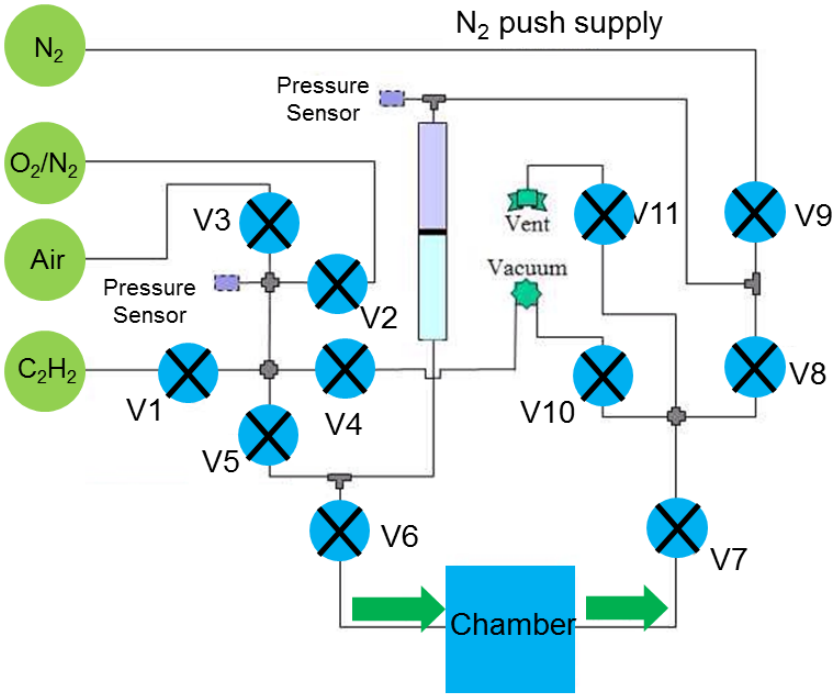

FIGURE 3.5: Schematic of the valves from Ref. [73].

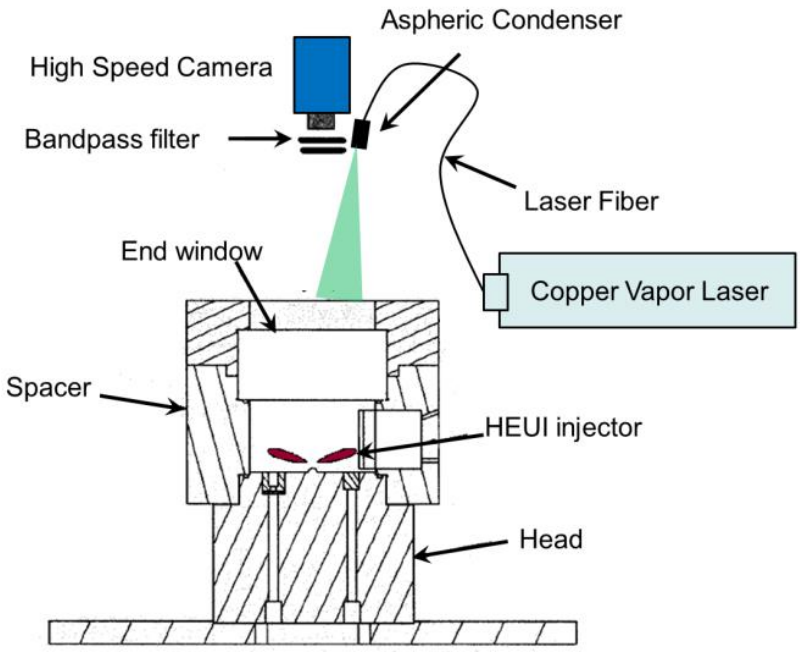

FIGURE 3.6: Schematic of the laser setup from Ref. [73].

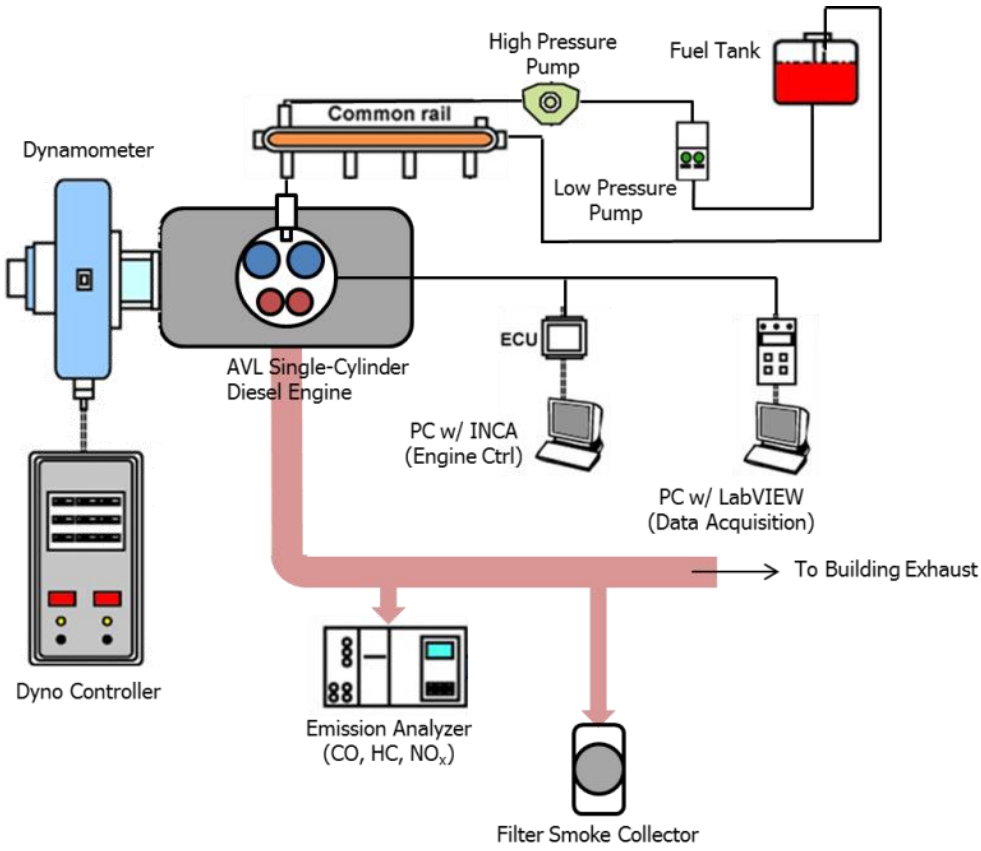

FIGURE 3.7: Experimental setup for the AVL diesel engine.

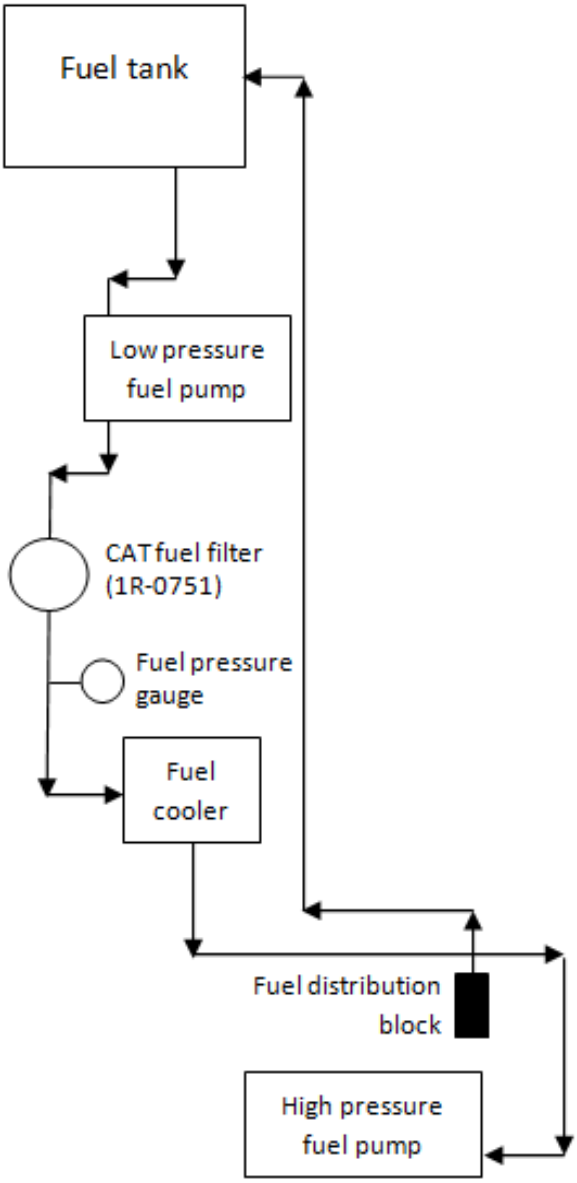

FIGURE 3.8: Low pressure fuel system.

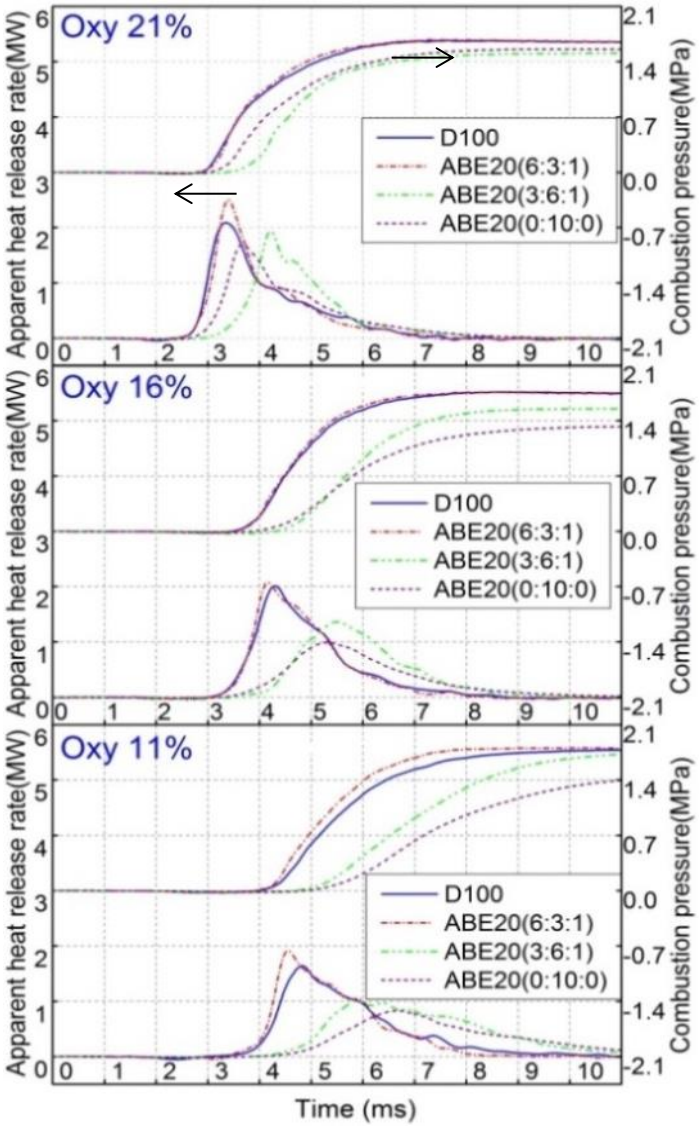

FIGURE 4.1: Pressure trace and apparent heat release rate of different ABE mixture blended with diesel, under ambient temperature of 800K and various ambient oxygen conditions. From Ref. [65].

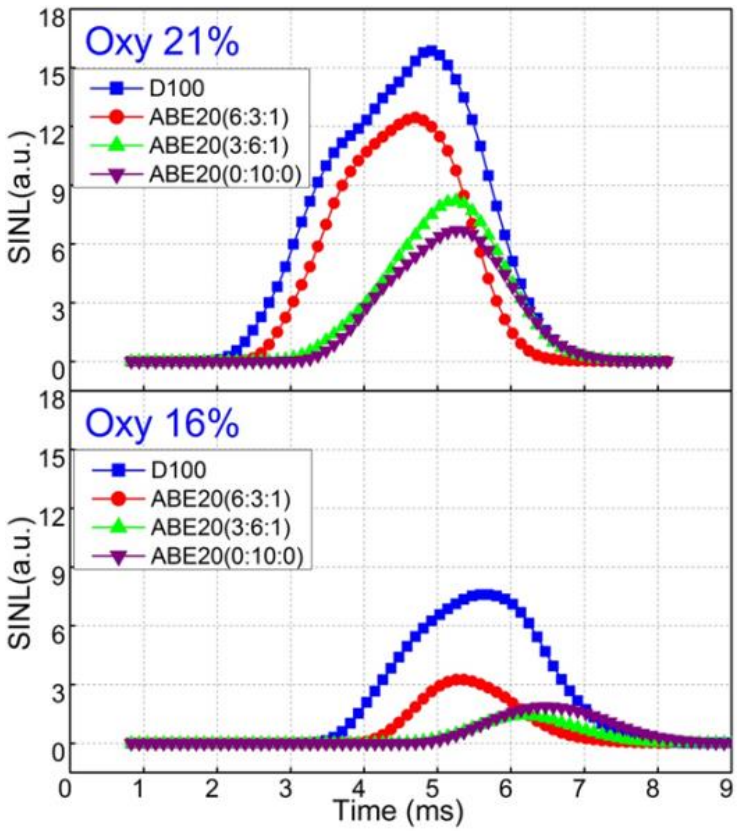

FIGURE 4.2: Spatial integrated natural flame luminosity (SINL) of different ABE mixture blended with diesel, under ambient temperature of 800K and ambient oxygen concentration of 21% and 16%. From Ref. [65].

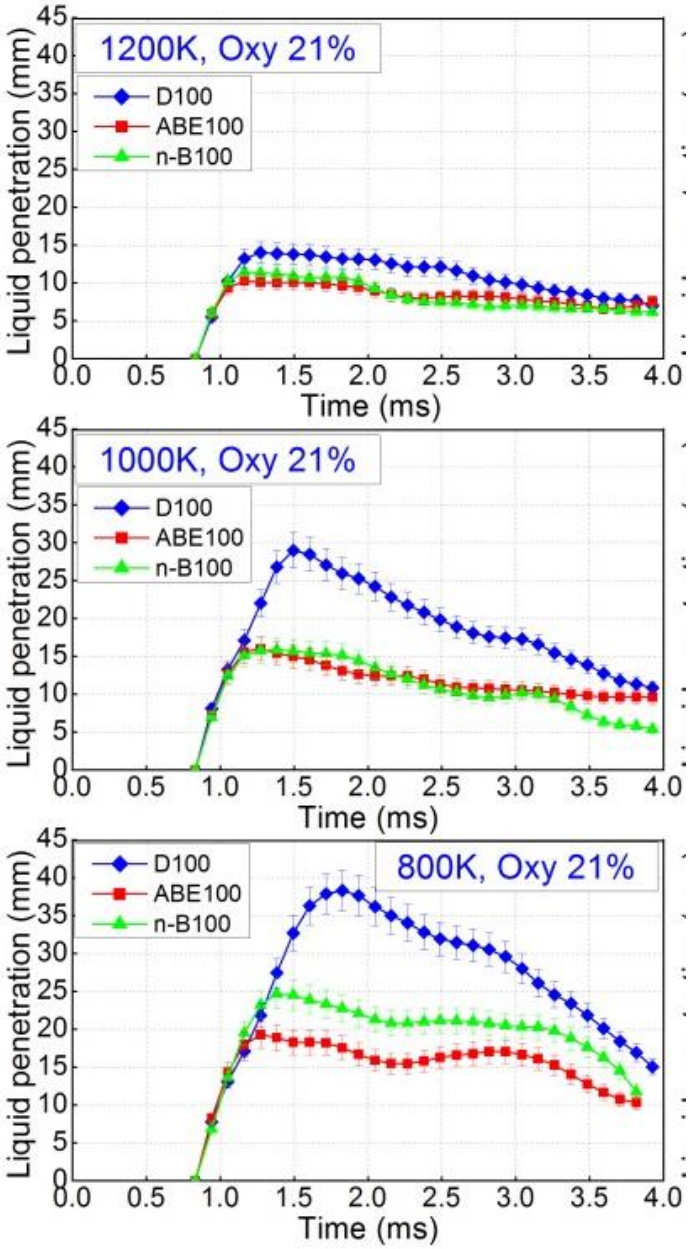

FIGURE 4.3: Liquid penetration length of pure diesel, ABE and pure butanol at different ambient temperature conditions. From Ref. [68]

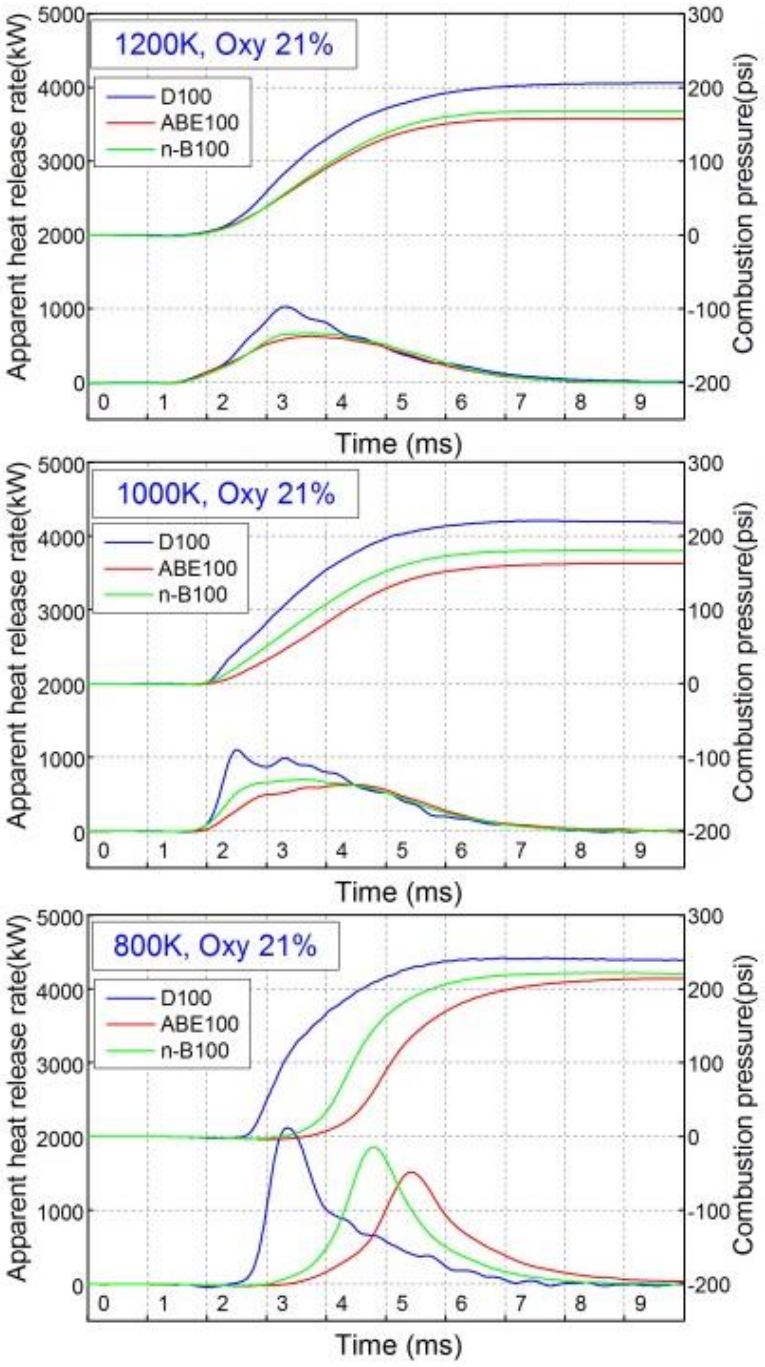

FIGURE 4.4: Combustion pressure trace and apparent heat release rate of pure diesel, ABE and pure butanol at different ambient temperature conditions. From Ref. [68]

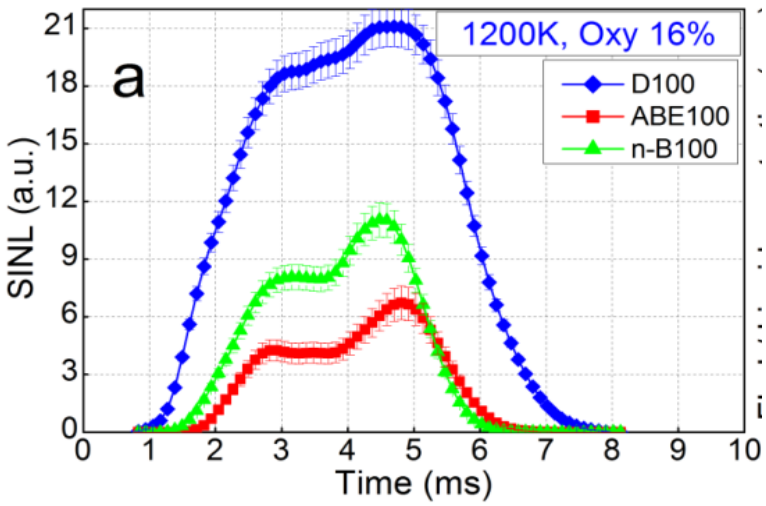

FIGURE 4.5: Spatial integrated natural flame luminosity of pure diesel, ABE and pure butanol at 1200K ambient temperature condition. From Ref. [68]

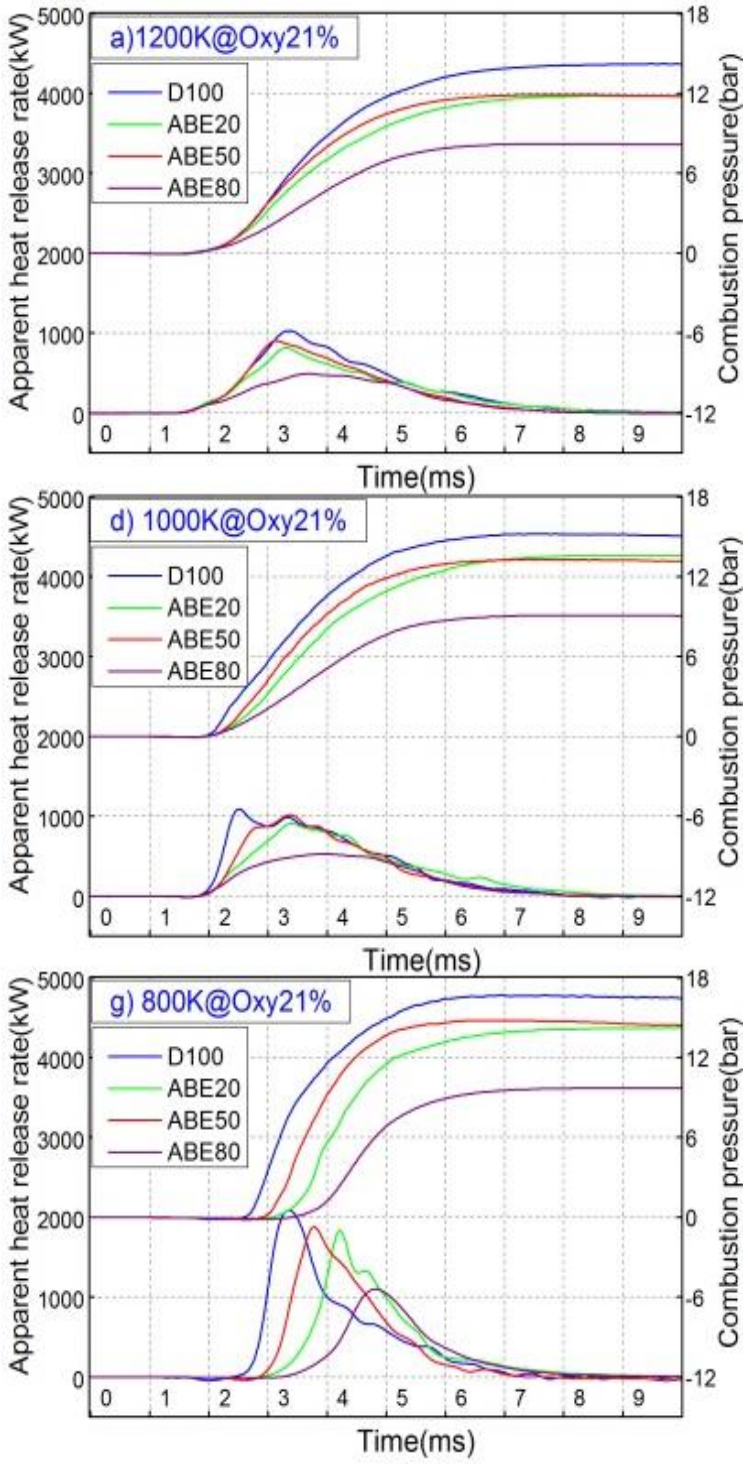

FIGURE 4.6: Combustion pressure and apparent heat release rate of ABE20, ABE50 and ABE80. From Ref. [71]

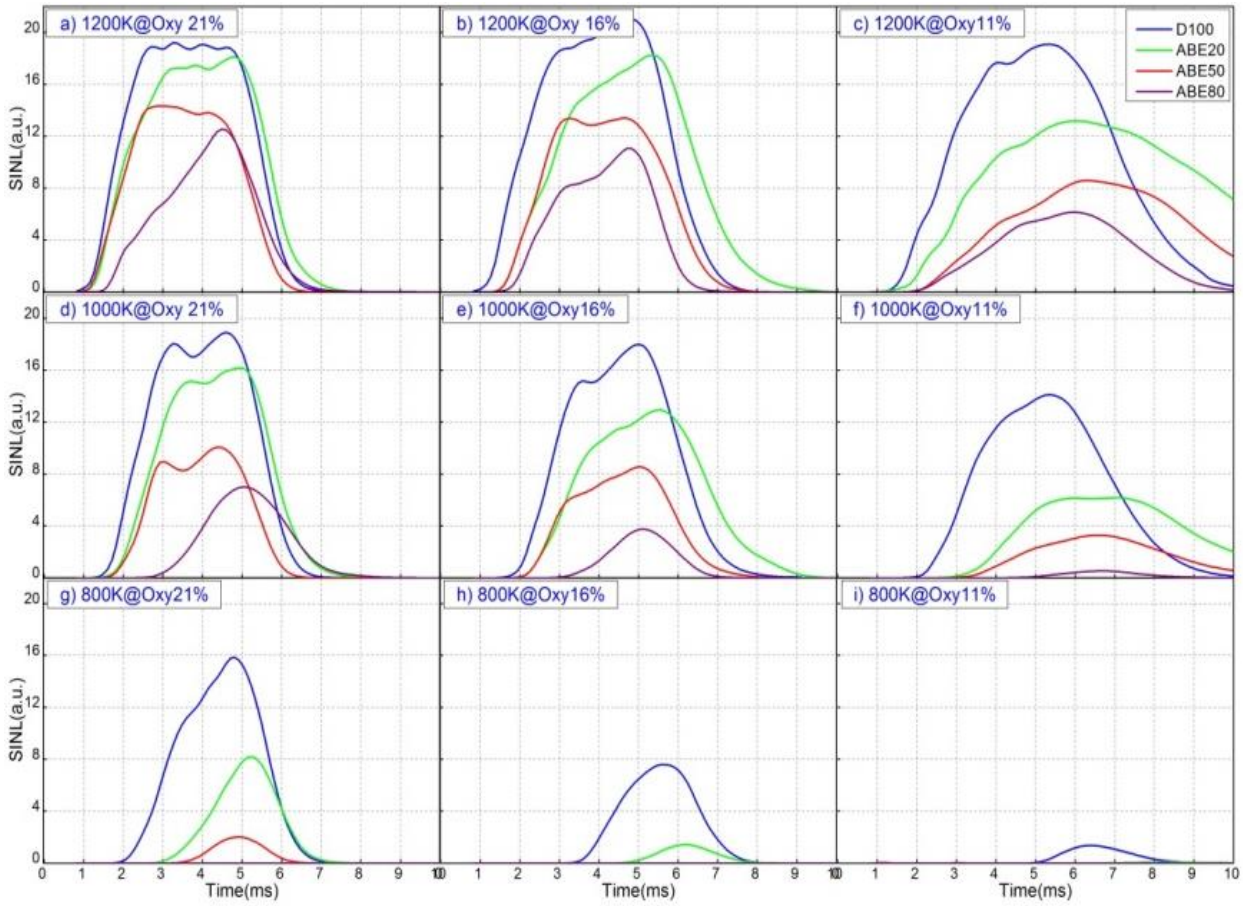

FIGURE 4.7: Spatial integrated natural flame luminosity of ABE20, ABE50, ABE100 and pure diesel in various temperature and ambient oxygen concentration conditions. From Ref. [71]

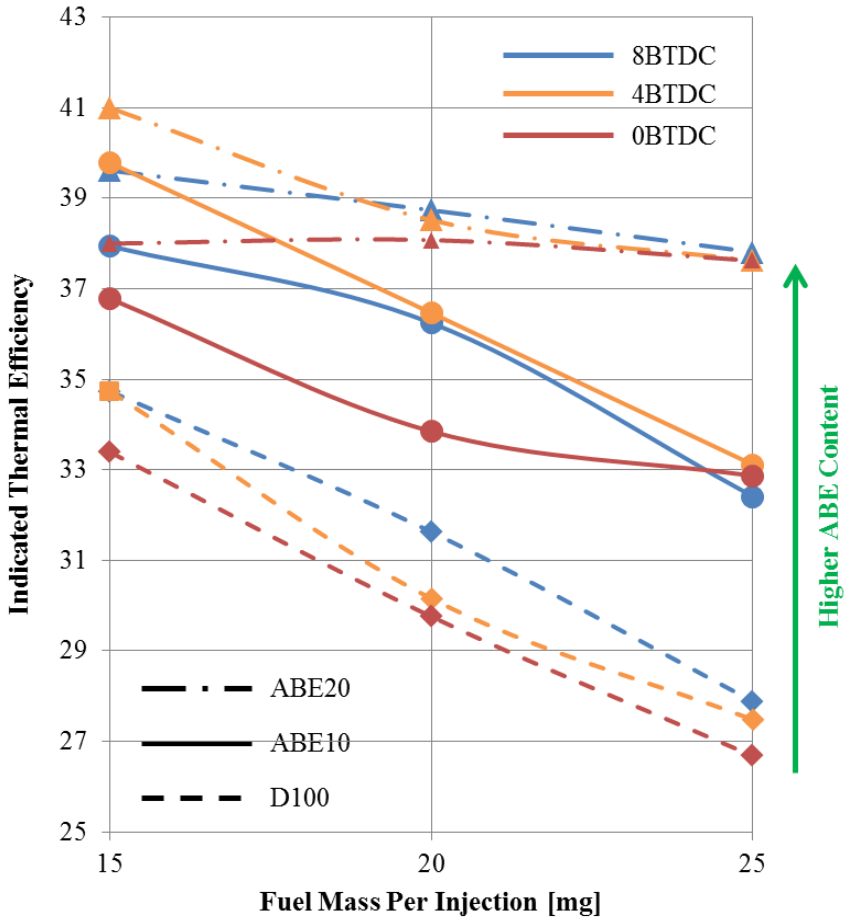

FIGURE 4.8: Indicated thermal efficiency of valid conditions tested.

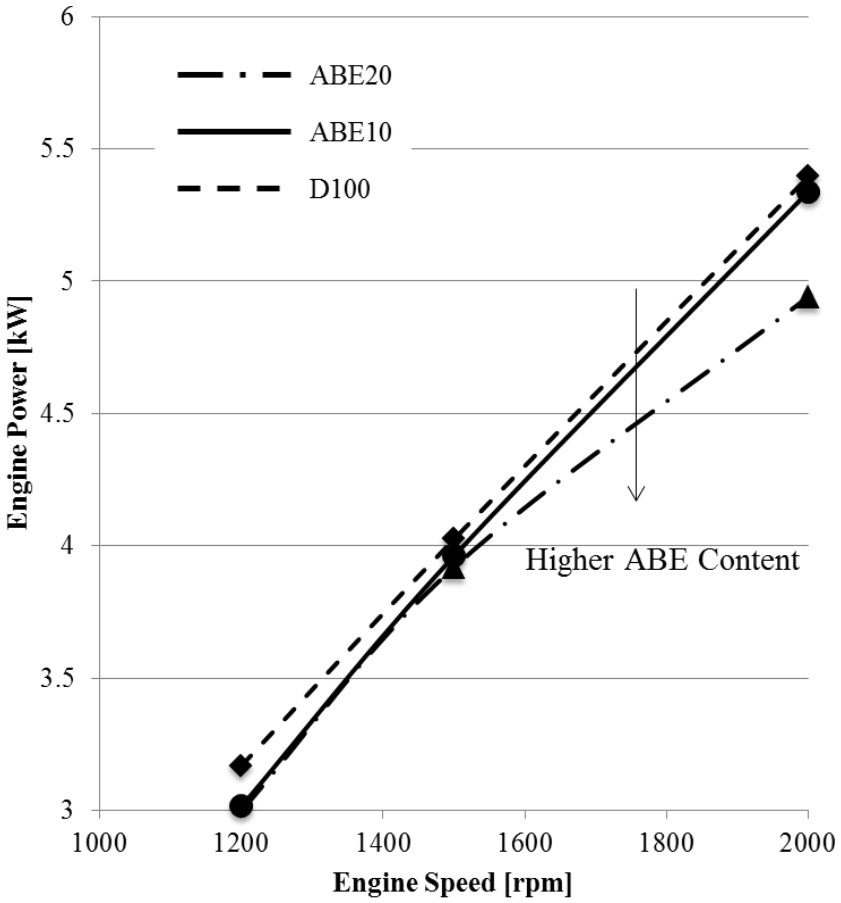

FIGURE 4.9: Engine power output of different fuels tested.

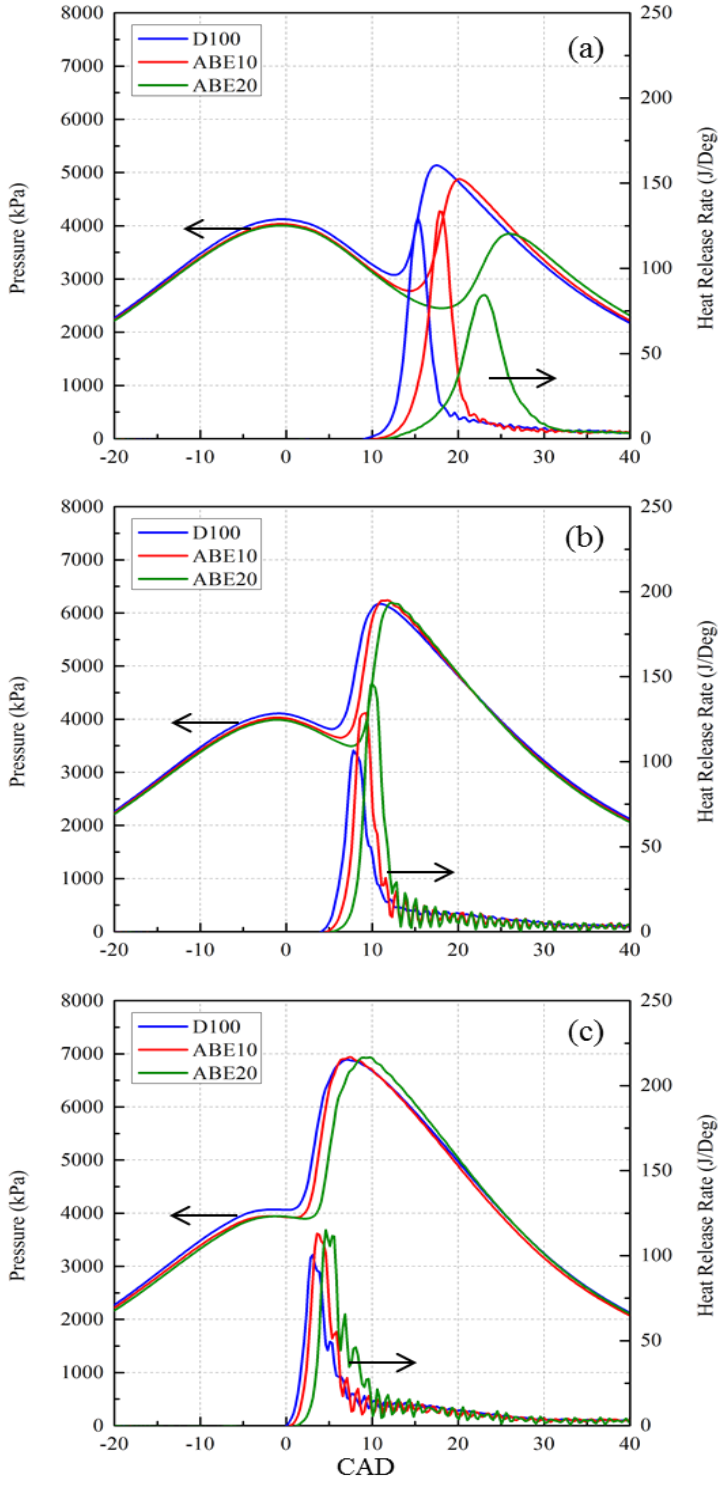

FIGURE 4.10: In-cylinder pressure trace and heat release rate at 1500 RPM and with an injection timing of: (a) 0 CAD BTDC; (b) 4 CAD BTDC; (c) 8 CAD BTDC

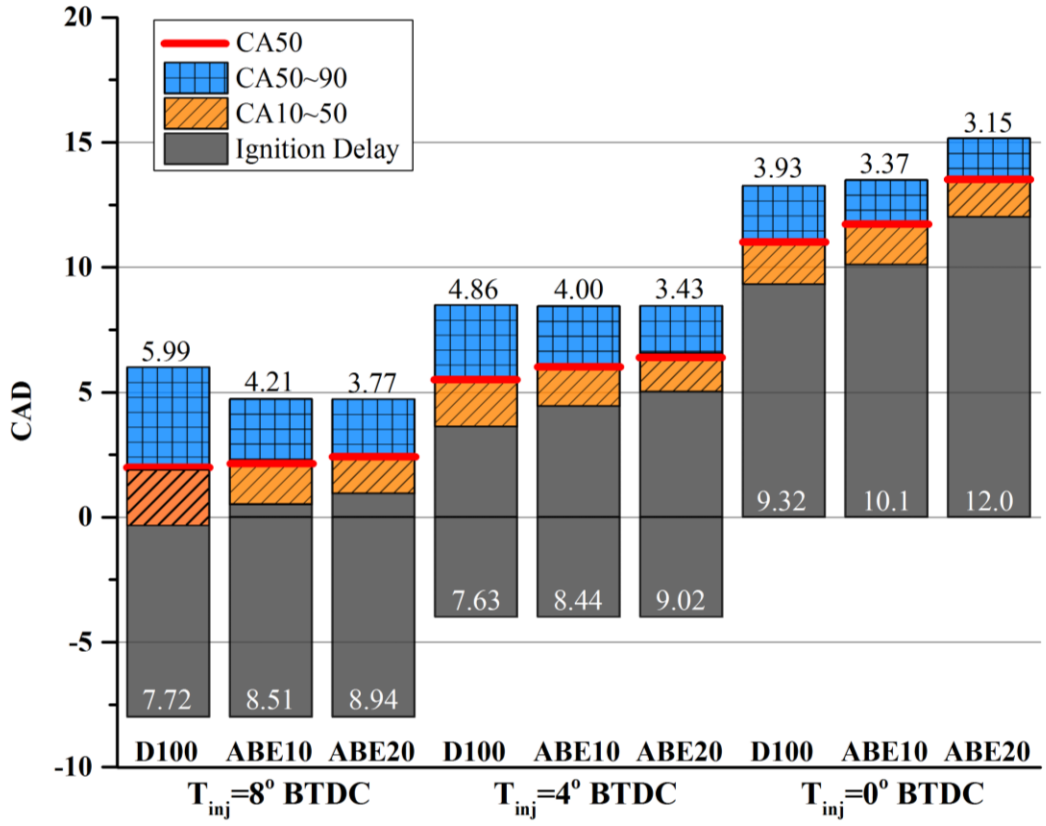

FIGURE 4.11: Combustion phasing diagram of the tested fuels at different injection timings. (1200RPM, 25mg fuel/stroke)

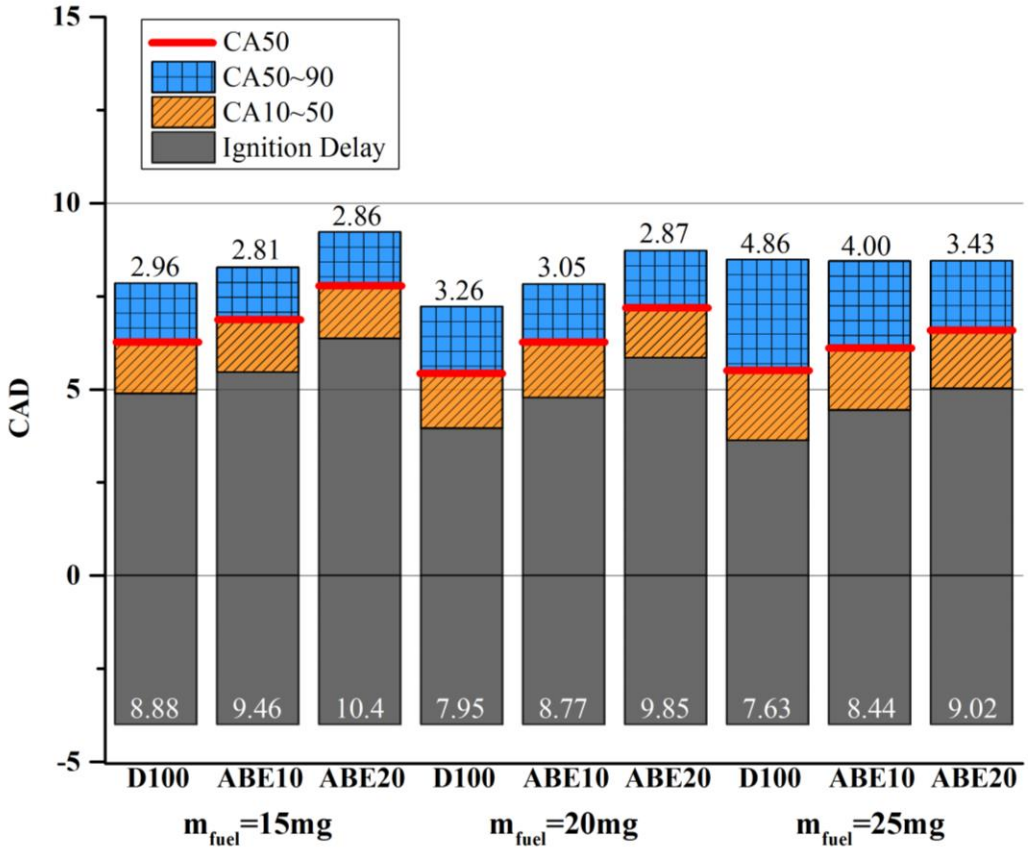

FIGURE 4.12: Combustion phasing diagram of the tested fuels at different load conditions. (1200RPM, 4CAD BTDC Injection Timing)

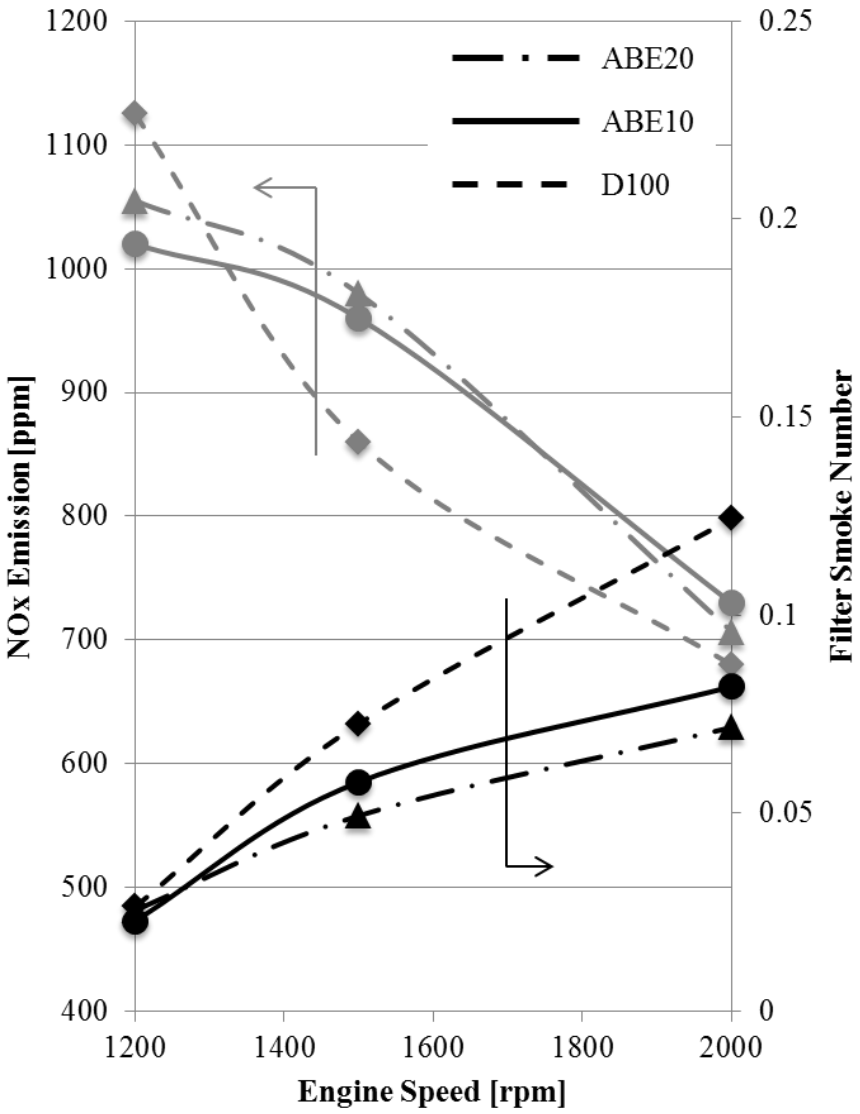

FIGURE 4.13: Trade-off relations between NOx and PM emissions.

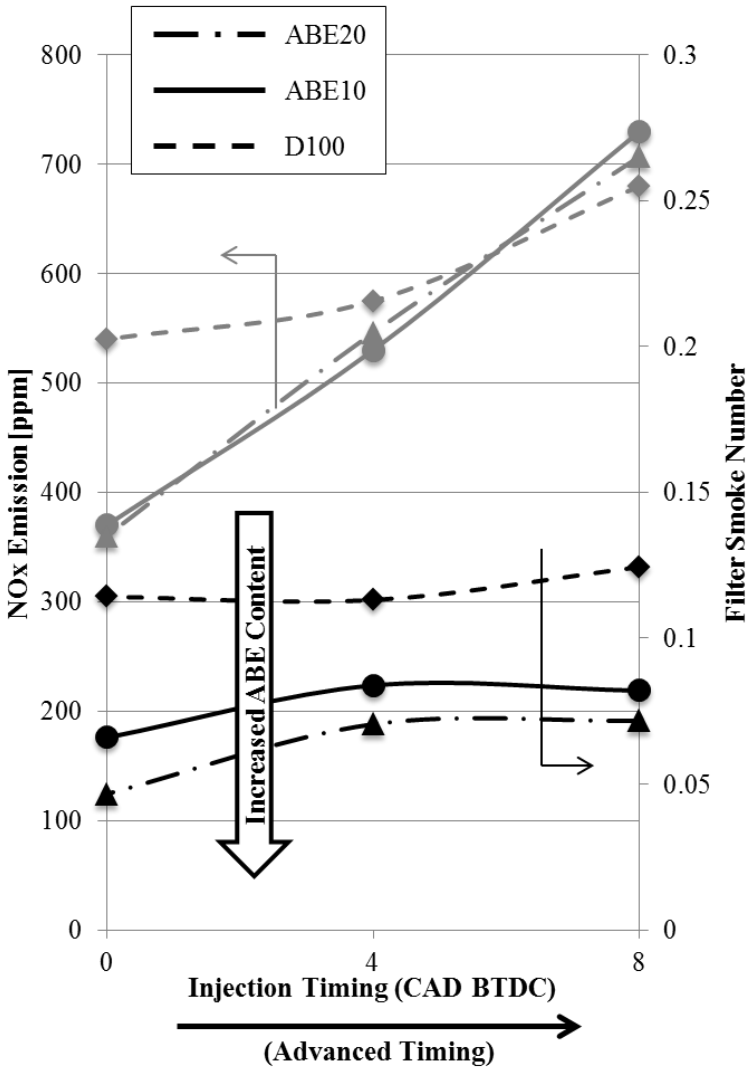

FIGURE 4.14: Injection timing sweep of soot and NO_x emission of tested fuels at engine speed of 2000RPM and 20 mg/injection.

References

1. Kumar, S., Cho, J.H., Park, J., Moon, I., "Advances in Diesel-Alcohol Blends and their Effects on the Performance and Emissions of Diesel Engines," *Renewable and Sustainable Energy Reviews* 22:46-72, 2013, doi: 10.1016/j.rser.2013.01.017.
2. Liu, F., Liu, L., Feng, X., "Separation of Acetone-Butanol-Ethanol (ABE) From Dilute Aqueous Solutions by Pervaporation," *Separation and Purification Technology* 42(3):273-282, 2005, doi:10.1016/j.seppur.2004.08.005.
3. García, V., Päkkilä, J., Ojamo, H., Muurinen, E., et al., "Challenges in Biobutanol Production: How to Improve Efficiency," *Renewable and Sustainable Energy Reviews* 15(2):964-980, 2011, doi:10.1016/j.rser.2010.11.008.
4. Hansen, Alan C., and Dimitrios C. Kyritsis. "Characteristics of Biofuels and Renewable Fuel Standards." *Biomass to Biofuels: Strategies for Global Industries* (2009): 1-26.
5. Qureshi, N., and H. P. Blaschek. "Recovery of Butanol from Fermentation Broth by Gas Stripping." *Renewable Energy* 22, no. 4 (2001): 557-564.
6. Qureshi, N. and H.P. Blaschek. "ABE Production from Corn: a Recent Economic Evaluation." *Journal of Industrial Microbiology and Biotechnology*, 2001. 27(5): p. 292-297.
7. Agathou, Maria S., Joshua W. Powell, F. Lee Chia-fon, and Dimitrios C. Kyritsis. "Preliminary Experimental Study of Butanol Electrosprays for Power Generation." *SAE Technical Paper* 2007-24-0020, 2007.
8. Ezeji, T.C., N. Qureshi and H.P. Blaschek. "Butanol Fermentation Research: Upstream and Downstream Manipulations." *The Chemical Record*, 2004. 4(5): p. 305-314.

9. Heywood, John B. *Internal Combustion Engine Fundamentals.* Vol. 930. New York: Mcgraw-hill, 1988.
10. Lapuerta, Magín, Reyes García-Contreras, Javier Campos-Fernández, and M. Pilar Dorado. "Stability, lubricity, viscosity, and cold-flow properties of alcohol− diesel blends." *Energy & Fuels* 24, no. 8 (2010): 4497-4502.
11. Lin, Yuan-Chung, Wen-Jhy Lee, How-Ran Chao, Shu-Li Wang, Tsui-Chun Tsou, Guo-Ping Chang-Chien, and Perng-Jy Tsai. "Approach for energy saving and pollution reducing by fueling diesel engines with emulsified biosolution/biodiesel/diesel blends." *Environmental science & technology* 42, no. 10 (2008): 3849-3855.
12. Rakopoulos, C. D., A. M. Dimaratos, E. G. Giakoumis, and D. C. Rakopoulos. "Study of turbocharged diesel engine operation, pollutant emissions and combustion noise radiation during starting with bio-diesel or n-butanol diesel fuel blends." *Applied Energy* 88, no. 11 (2011): 3905-3916.
13. Andrae, Johan CG. "Development of a detailed kinetic model for gasoline surrogate fuels." *Fuel* 87.10 (2008): 2013-2022.
14. Thurber, Mark C., Frederic Grisch, Brian J. Kirby, Martin Votsmeier, and Ronald K. Hanson. "Measurements and modeling of acetone laser-induced fluorescence with implications for temperature-imaging diagnostics." *Applied Optics* 37, no. 21 (1998): 4963-4978.
15. Braeuer, Andreas, Frank Beyrau, and Alfred Leipertz. "Laser-induced fluorescence of ketones at elevated temperatures for pressures up to 20 bars by using a 248 nm excitation laser wavelength: experiments and model improvements." *Applied Optics* 45, no. 20 (2006): 4982-4989.

16. Koban, W., J. D. Koch, Volker Sick, N. Wermuth, R. K. Hanson, and Christof Schulz. "Predicting LIF signal strength for toluene and 3-pentanone under engine-related temperature and pressure conditions." *Proceedings of the Combustion Institute* 30, no. 1 (2005): 1545-1553.
17. Wu, Fujia, and Chung K. Law. "An experimental and mechanistic study on the laminar flame speed, Markstein length and flame chemistry of the butanol isomers." *Combustion and Flame* 160, no. 12 (2013): 2744-2756.
18. Liu, Haifeng, Chia-fon F. Lee, Ming Huo, and Mingfa Yao. "Combustion characteristics and soot distributions of neat butanol and neat soybean biodiesel." *Energy & Fuels* 25, no. 7 (2011): 3192-3203.
19. Liu, Haifeng, Chia-Fon Lee, Yu Liu, Ming Huo, and Mingfa Yao. "Spray and combustion characteristics of n-butanol in a constant volume combustion chamber at different oxygen concentrations." *SAE Technical Paper* 2011-01-1190, 2011.
20. Liu, Yu, Jun Li, Ying Gao, and Xinmei Yuan. "Laser Diagnostic Investigation on the Spray and Combustion with Butanol-Biodiesel-Diesel Fuel Blends." *Advanced Materials Research Vols.443-444* (2012): 986-995.
21. Liu, Yu, Jun Li, Ying Gao, and Xinmei Yuan. "Analysis of Micro-Explosion Phenomenon in a Constant Volume Chamber by Butanol-Biodiesel-Diesel Blend Fuel." *Advanced Materials Research Vols.443-444* (2012): 996-1006.
22. Liu, Yu, Jun Li, Ying Gao, and Xinmei Yuan. "Experimental Study on Spray Characteristics of N-butanol/ Acidic Oil/Diesel Blends." *Advanced Materials Research Vols.1008-1009* (2014): 1001-1005.

23. Liu, Haifeng, et al. "Comparison of ethanol and butanol as additives in soybean biodiesel using a constant volume combustion chamber." *Energy & fuels* 25.4 (2011): 1837-1846.
24. Hansen, Alan C., Qin Zhang, and Peter WL Lyne. "Ethanol–diesel fuel blends—a review." *Bioresource technology* 96.3 (2005): 277-285.
25. Hu, Chen, et al. "Effects of ethanol in ester-ethanol-diesel blended fuels on spray behavior and PM emission." No. 2006-01-0236. *SAE Technical Paper*, 2006.
26. Nithyanandan, K., Wu, H., Huo, M., and Lee, C., "A Preliminary Investigation of the Performance and Emissions of a Port-Fuel Injected SI Engine Fueled with Acetone-Butanol-Ethanol (ABE) and Gasoline," *SAE Technical Paper* 2014-01-1459, 2014, doi:10.4271/2014-01-1459.
27. Nithyanandan, K., Wu, H., Zhang, J., and Lee, C. F., "Performance and Emissions of Acetone-Butanol-Ethanol (ABE) and Gasoline Blends in a Port Fuel Injected Spark Ignition Engine", Proc. *ASME. 46162; Volume 1: Large Bore Engines; Fuels; Advanced Combustion; Emissions Control Systems*, V001T02A010.October 19, 2014, ICEF2014-5644, doi: 10.1115/ICEF2014-5644.
28. Nithyanandan, K., Zhang, J., Yuqiang, L., Wu, H. et al., "Investigating the Impact of Acetone on the Performance and Emissions of Acetone-Butanol-Ethanol (ABE) and Gasoline Blends in an SI Engine," *SAE Technical Paper* 2015-01-0909, 2015, doi:10.4271/2015-01-0909.
29. Zhang, J., Nithyanandan, K., Li, Y., Lee, C. et al., "Comparative Study of High-Alcohol-Content Gasoline Blends in an SI Engine," *SAE Technical Paper* 2015-01-0891, 2015, doi:10.4271/2015-01-0891.

30. Li, Y., Nithyanandan, K., Zhang, J., Lee, C. et al., "Combustion and Emissions Performance of a Spark Ignition Engine Fueled with Water Containing Acetone-Butanol-Ethanol and Gasoline Blends," *SAE Technical Paper* 2015-01-0908, 2015, doi:10.4271/2015-01-0908.
31. Chang, Yu-Cheng, et al. "Green energy: Water-containing acetone–butanol–ethanol diesel blends fueled in diesel engines." *Applied Energy* 109 (2013): 182-191.
32. Chang, Yu-Cheng, Wen-Jhy Lee, Tser Son Wu, Chang-Yu Wu, and Shui-Jen Chen. "Use of Water Containing Acetone–butanol–ethanol for NOx-PM (nitrogen Oxide-particulate Matter) Trade-off in the Diesel Engine Fueled with Biodiesel." *Energy* 64 (2014): 678-87.
33. Zhou, Nan, Han Wu, Chia-Fon Lee, Qingnian Wang, Ming Huo, and Pengyu Wang. "Different Percentage of Acetone-Butanol-Ethanol (ABE) and Diesel Blends at Low Temperature Condition in a Constant Volume Chamber." *SAE Technical Paper* 2014-01-1257, 2014.
34. Zhou, Nan, Ming Huo, Han Wu, Karthik Nithyanandan, Chia-fon F. Lee, and Qingnian Wang. "Low temperature spray combustion of acetone–butanol–ethanol (ABE) and diesel blends." *Applied Energy* 117 (2014): 104-115.
35. Depcik C., Jacobs T., Hagena J., & Assanis D. "Instructional use of a single-zone, premixed charge, spark-ignition engine heat release simulation." *International Journal of Mechanical Engineering Education*, 35 (1), 1 – 31, 2007.
36. Bowman C.T. "Control of combustion-generated nitrogen oxide emissions: technology driven by regulation." *Twenty-Fourth Symposium (International) on Combustion*, The Combustion Institute, 859-878, 1992.

37. Richter H. & Howard J.B. "Formation of polycyclic aromatic hydrocarbon and their growth to soot - a review of chemical reaction pathways." *Progress in Energy and Combustion Science 26*, 565-608, 2000.

38. Mansurov Z.A. "Soot formation in combustion process." *Combustion, Explosion, and Shock Waves* 41 (6), 727-744, 2005.

39. Maricq M. Chemical "Characterization of particulate emissions from diesel engines: a review." *Aerosol Science* 38, 1079-1118, 2007.

40. Hildemann L.M., Markowski G.R., & Cass G.R. "Chemical composition of emissions from urban sources of fine organic aerosol." *Environmental Science & Technology*, 25, 744–759, 1991.

41. D.L. Siebers. "Scaling Liquid-Phase Fuel Penetration in Diesel Sprays Based on Mixing Limited Vaporization." *SAE*. 1999-01-0528, 1999.

42. J.D. Naber, D.L. Siebers. "Effect of gas density and vaporization on penetration and dispersion of diesel sprays." *SAE*. 960034, 1996.

43. C. Espey, J. Dec. "The Effect of TDC Temperature and Density on the Liquid-Phase Fuel Penetration in a D.I. Diesel Engine." *SAE*. 952456, 1995.

44. S. Martinez-Martinez F.A. Sanchez-Cruz V.R. Bermudez J.M. Riesco-Avila. "Liquid Spray Characteristics in Diesel Engines." *In: Siano D*, Fuel Injection. InTech; 2010.

45. B.T. Fisher, C.J. Mueller. "Liquid Penetration Length of Heptamethylnonane and Trimethylpentane under Unsteady In-Cylinder Conditions." *Fuel*. 89(10):2673-2696, 2010.

46. C.L. Genzale, L.M. Pickett, S. Kook. "Liquid Penetration of Diesel and Biodiesel Sprays at Late-Cycle Post-Injection Conditions." *SAE*. 2010-01-0610, 2010.

47. L.M. Pickett, S. Kook, Williams TC. “Visualization of Diesel Spray Penetration, Cool-Flame, Ignition, High-Temperature Combustion, and Soot Formation Using High Speed Imaging.” *SAE*. 2009-01-0658, 2009.
48. S. Kook, L.M. Pickett, Musculus MPB. “Influence of Diesel Injection Parameters on End-of-Injection Liquid Length Recession.” *SAE*. 2009-01-1356, 2009.
49. B.S. Higgins, C.J. Mueller, D.L. Siebers. “Measurements of Fuel Effects on Liquid-Phase Penetration in DI Sprays.” *SAE*. 1999-01-0519, 1999.
50. D.L. Siebers, B. Higgins. “Flame Lift-Off on Direct-Injection Diesel Sprays under Quiescent Conditions.” *SAE*. 2001-01-0530. 2001.
51. B. Higgins, D.L. Siebers. “Measurement of the Flame Lift-Off Location on DI Diesel Sprays using OH Chemiluminescence.” *SAE*. 2001-01-0918, 2001.
52. L.M. Pickett, D.L. Siebers, C.A. Idicheria. “Relationship Between Ignition Processes and the Lift-off Length of Diesel Fuel Jets.” *SAE* 2005-01-3843, 2005.
53. H. Kosaka, T. Aizawa, T. Kemimoto. “Two dimensional imaging of ignition and soot formation processes in a diesel flame.” *International Journal of Engine Research*, 6, 21-42, 2005.
54. J. Dec, D. Tree. “Diffusion-flame/wall interactions in a heavy duty diesel engine.” *SAE Technical Paper*, 2001-01-1295, 2001.
55. M. Bakenhus, R. Reitz. “Two-color combustion visualization of single and split injections in a single-cylinder heavy-duty D.I. diesel engine using an endoscope based imaging system.” *SAE Technical Paper*, 1999-01-1112.

56. M.P.B. Musculus, J.E. Dec, D.R. Tree, D. Daly, D. Langer, T.W. Ryam, et al., "Effects of Water Fuel Emulsions on Spray and Combustion Processes in a heavy-duty DI diesel engine." *SAE* 2003-01-3146, 2003.

57. H. Zhao, N. Ladommatos. "Optical diagnostic for soot and temperature measurements in diesel engines." *Prog. Energy Combust. Sci*. 24, 221-255, 1998.

58. L.M. Pickett, "Low flame temperature limits for mixing-controlled diesel combustion." *Proceedings of the Combustion Institute* 30, 2727-2735, 2005.

59. S.B. Kook, P.C. Miles, D. Choi, L.M. Pickett, "The Influence of Charge Dilution and Injection Timing on Low-Temperature Diesel Combustion and Emissions." *SAE* 2005-01-3837, 2005.

60. M.P.B. Musculus, L.M. Pickett. "Diagnostic considerations for optical laser-extinction measurements of soot in high-pressure transient combustion environments." *Combustion and Flame*, 141, 371-391, 2005.

61. S. Kook, L.M. Pickett. "Soot volume fraction and morphology of conventional and surrogate jet fuel sprays at 1000K and 6.7MPa ambient conditions." *Proceedings of the Combustion Institute*, 33 2911-2918, 2011.

62. L.M. Pickett, D.L. Siebers. "An Investigation of Diesel Soot Formation Processes using Micro-Orifices." *Proceedings of the Combustion Institute*. 29(1):655-662, 2002.

63. L.M. Pickett, D.L. Siebers. "Soot in diesel fuel jets: effects of ambient temperature, ambient density, and injection pressure." *Combustion and Flame*, 138, 114-135, 2004.

64. Y. Xu. "Investigation of clean diesel combustion with oxygenated fuels in a constant volume chamber using forward illumination light extinction techniques." PhD Dissertation, University of Illinois at Urbana Champaign, 2006.

65. Wu, Han, Karthik Nithyanandan, Nan Zhou, Timothy H. Lee, F. Lee Chia-fon, and Chunhua Zhang. "Impacts of acetone on the spray combustion of Acetone–Butanol–Ethanol (ABE)-Diesel blends under low ambient temperature." *Fuel* (2014).
66. Wu, Han, Ming Huo, Nan Zhou, Karthik Nithyanandan, Chia-Fon Lee, Chunhua Zhang, and Jiang Lin. "An Experimental Investigation of the Combustion Characteristics of Acetone-Butanol-Ethanol-Diesel Blends with Different ABE Component Ratios in a Constant Volume Chamber." *SAE Technical Paper* 2014-01-1452, 2014.
67. Dec, John, "A Conceptual Model of DI Diesel Combustion Based on Laser-Sheet Imaging," *SAE Technical Paper* 970873, 1997.
68. Wu, Han, Karthik Nithyanandan, Timothy H. Lee, Chia-fon F. Lee, and Chunhua Zhang. "Spray and Combustion Characteristics of Neat Acetone-Butanol-Ethanol (ABE), n-Butanol and Diesel in a Constant Volume Chamber." *Energy & Fuels*, 2014 *28* (10), 6380-6391.
69. Pickett, Lyle M., Dennis L. Siebers, and Cherian A. Idicheria. "Relationship between ignition processes and the lift-off length of diesel fuel jets," *SAE Technical Paper* 2005-01-3843, 2005.
70. Wu, Han, Karthik Nithyanandan, Boqi Li, Timothy H. Lee, Chia-fon F. Lee and Chunhua Zhang. "Investigation on Spray and Soot Lift-off Length of An ABE-Diesel Blend in A Constant Volume Chamber With Diesel Engine Conditions." *Proceedings of the ASME 2014 Internal Combustion Engine Division Fall Technical Conference*, American Society of Mechanical Engineers, 2014.
71. Wu, Han, Karthik Nithyanandan, Jiaxiang Zhang, Yilu Lin, Timothy H. Lee, Chia-fon F. Lee, Chunhua Zhang. "Impacts of Acetone-Butanol-Ethanol (ABE) Ratios on Spray and Combustion Characteristics of ABE-Diesel Blends," *Applied Energy*, Accepted, In Press.

72. Lin, Yilu, Han Wu, Karthik Nithyanandan, Timothy H. Lee, Chia-fon Lee and Chunhua Zhang. “Investigation of High Percentage Acetone-Butanol-Ethanol (ABE) Blended with Diesel in a Constant Volume Chamber.” *Proceedings of the ASME 2014 Internal Combustion Engine Division Fall Technical Conference*, American Society of Mechanical Engineers, 2014.
73. Hou, M., “Air/Fuel Mixing Enhancement and Emission Reduction Through Intake Port Design and Various Fuel Emulsions for Diesel Combustion”, PhD Thesis, Department of Mechanical Science and Engineering. Urbana, IL, University of Illinois at Urbana-Champaign, 2014.
74. Leick, M., “Optimizing conventional combustion and implementing low temperature combustion of biodiesel in a common-rail high-speed direct-injection engine”, MS Thesis, Department of Mechanical Science and Engineering. Urbana, IL, University of Illinois at Urbana-Champaign, 2010.
75. Chang, Yu-Cheng, Wen-Jhy Lee, Tser Son Wu, Chang-Yu Wu, and Shui-Jen Chen. "Use of Water Containing Acetone–Butanol–Ethanol for NOx-PM (Nitrogen Oxide-Particulate Matter) Trade-off in the Diesel Engine Fueled with Biodiesel." *Energy* 64 (2014): 678-87.